

Aligning Few-Step Diffusion Models with Dense Reward Difference Learning

Ziyi Zhang¹ Li Shen² Sen Zhang³ Deheng Ye⁴
 Yong Luo^{1*} Miaojing Shi⁵ Bo Du¹ Dacheng Tao⁶

¹Wuhan University ²Sun Yat-Sen University ³ByteDance Inc.

⁴Tencent Inc. ⁵Tongji University ⁶Nanyang Technological University

{ziyizhang27, luoyong, dubo}@whu.edu.cn {mathshenli, dacheng.tao}@gmail.com

sen.zhang@sydney.edu.au dericye@tencent.com mshi@tongji.edu.cn

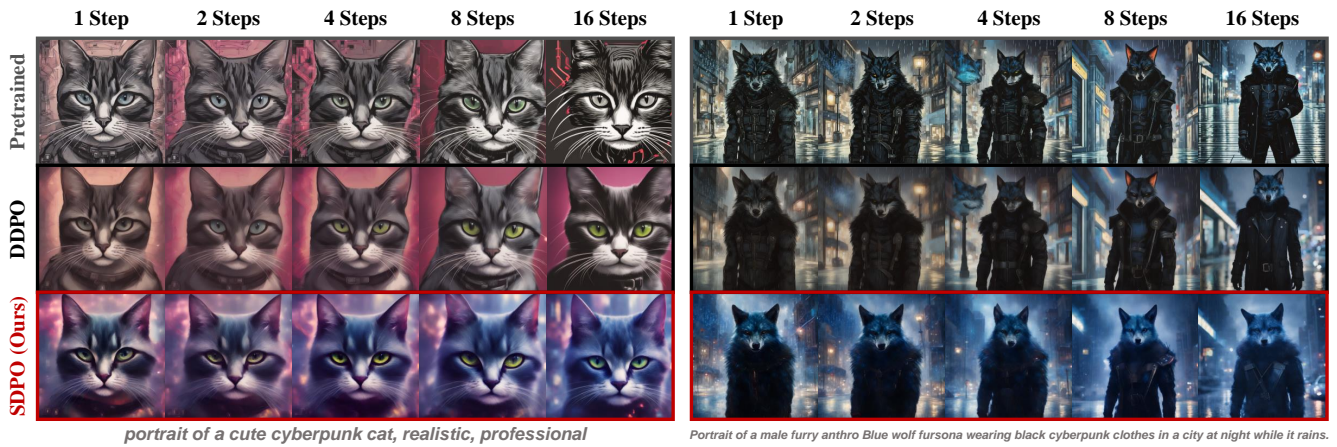


Figure 1. Generated images for unseen prompts by: a pretrained few-step diffusion model (SD-Turbo [42]), and models finetuned with DDPO [1] and our SDPO, both using PickScore [17] and the same number of training samples. SDPO consistently delivers high-quality, reward-aligned images across various sampling step settings. All images are generated using the same random seed.

Abstract

Aligning diffusion models with downstream objectives is essential for their practical applications. However, standard alignment methods often struggle with step generalization when directly applied to few-step diffusion models, leading to inconsistent performance across different denoising step scenarios. To address this, we introduce Stepwise Diffusion Policy Optimization (SDPO), a novel alignment method tailored for few-step diffusion models. Unlike prior approaches that rely on a single sparse reward from only the final step of each denoising trajectory for trajectory-level optimization, SDPO incorporates dense reward feedback at every intermediate step. By learning the differences in dense rewards between paired samples, SDPO facilitates stepwise optimization of few-step diffusion models, ensuring consistent alignment across all denoising steps. To promote stable and efficient training, SDPO introduces an online reinforcement learning framework featuring several

novel strategies designed to effectively exploit the stepwise granularity of dense rewards. Experimental results demonstrate that SDPO consistently outperforms prior methods in reward-based alignment across diverse step configurations, underscoring its robust step generalization capabilities. Code is available at <https://github.com/ZiyiZhang27/sdpo>.

1. Introduction

While text-to-image diffusion models [6, 35, 40, 45] excel at generating high-resolution images from text prompts, they often suffer from slow generation speed due to their iterative denoising processes. Recent approaches [16, 25, 27–29, 31, 33, 41, 42, 47, 57, 58] have shown promise in distilling standard multi-step diffusion models into *few-step* generators, significantly reducing the number of denoising steps required to produce appealing, high-resolution im-

ages. However, these few-step diffusion models may not inherently align with specific downstream objectives, such as aesthetic quality [43] or user preferences [17, 23, 51, 54].

A promising approach to address this alignment problem for multi-step diffusion models is *reinforcement learning (RL)-based finetuning* [1, 7, 8], which enables model optimization toward downstream reward functions. However, these methods typically assume a fixed number of steps for each denoising trajectory. When applied to finetune models on few-step trajectories (e.g. 1 to 4 steps), they often result in training instability and sample inefficiency. Conversely, using the standard step settings (e.g. 20 to 50 steps) of these methods can lead to *step generalization* issues, where models overfit to specific trajectory lengths, impairing their few-step inference ability. A key factor in this issue is the *sparse* reward feedback from only the final denoising step, causing models to overly focus on the final image quality while neglecting the intermediate steps. However, deriving *dense* rewards for each step is challenging, as existing reward functions are typically based on the distributions of final clean images rather than the intermediate noisy samples.

In this work, we propose *Stepwise Diffusion Policy Optimization* (SDPO), an RL algorithm that aligns few-step diffusion models by learning dense reward differences between paired samples in a stepwise manner. Specifically, SDPO provides continuous, dense reward feedback throughout the entire denoising trajectory by utilizing predicted original samples from each intermediate step, rather than focusing solely on the final output. To obtain this dense reward feedback efficiently, we develop a latent similarity-based reward prediction strategy. This strategy adaptively selects key reward query steps within each trajectory, predicting dense rewards for the remaining steps based on latent similarity, minimizing computational cost.

By incorporating dense reward feedback at each denoising step, SDPO distinguishes itself from traditional reward difference-based methods [5, 9], which typically rely on the difference of final-step rewards for trajectory-level optimization. Instead, SDPO facilitates stepwise optimization based on the differences of dense rewards, reducing the risk of overfitting to sparse, final-step rewards and promoting consistent alignment across all denoising steps. To ensure a stable and efficient optimization process, SDPO introduces an online RL framework featuring several novel strategies, such as per-step-prompt reward normalization, stepwise importance weighting, and step-shuffled gradient updates—each specifically designed to effectively exploit the stepwise granularity of our dense reward predictions.

Our experiments show that SDPO demonstrates superior sample efficiency in finetuning few-step diffusion models and exhibits strong step generalization in post-training evaluations, consistently achieving high reward scores and delivering reward-aligned images across diverse sampling step

settings. Our contributions are summarized as follows:

- We propose SDPO, which addresses step generalization in aligning few-step diffusion models for the first time. By incorporating dense reward feedback throughout the denoising process, SDPO facilitates stepwise diffusion policy optimization based on dense reward differences.
- To efficiently provide dense rewards, we develop a latent similarity-based reward prediction strategy, ensuring dense feedback without excessive computational cost.
- We design a novel online RL framework for SDPO, with several key innovations that effectively exploit dense rewards, facilitating more stable and efficient optimization.
- We validate SDPO’s effectiveness in improving step generalization through comprehensive experiments, showing consistent alignment across diverse step configurations.

2. Preliminaries

2.1. Diffusion Models

Denoising diffusion probabilistic models [12] generate high-quality samples by iteratively transforming noise into complex data distributions through a denoising process. In text-to-image applications, these models typically condition each denoising step on a text prompt \mathbf{c} that describes the desired image, and are operated in two key phases: a forward process that gradually adds noise to an initial sample \mathbf{x}_0 at each step $t \in \{1, \dots, T - 1\}$, resulting in progressively noisier samples \mathbf{x}_t ; and a reverse process that estimates the conditional distribution $p_\theta(\mathbf{x}_{t-1}|\mathbf{x}_t, \mathbf{c})$ at each step, iteratively removing noise to recover the original data.

In the reverse process, each denoising step t produces an estimate of the underlying clean sample $\hat{\mathbf{x}}_t$, often referred to as the *predicted original sample*, or the *denoised sample*. At each step t , given a noisy input \mathbf{x}_t , the model predicts the noise component $\epsilon_\theta(\mathbf{x}_t, t, \mathbf{c})$, which represents the noise present in the current sample. Using this noise estimate, the model computes the predicted original sample $\hat{\mathbf{x}}_t$, as:

$$\hat{\mathbf{x}}_t = (\mathbf{x}_t - \sqrt{1 - \bar{\alpha}_t} \cdot \epsilon_\theta(\mathbf{x}_t, t, \mathbf{c})) / \sqrt{\bar{\alpha}_t}, \quad (1)$$

where $\bar{\alpha}_t$ is the cumulative product of the noise scaling factors α_t up to step t . The quality of these intermediate predictions progressively improves as denoising continues.

2.2. Reinforcement Learning for Diffusion Models

Denoising as a Markov decision process (MDP). To perform RL-based finetuning for diffusion models, prior works [1, 8] formulate the denoising process of diffusion models as a T -step MDP, which is defined as follows:

$$s_t \triangleq (\mathbf{c}, \mathbf{x}_{T-t}), \quad a_t \triangleq \mathbf{x}_{T-t-1}, \quad (2)$$

$$\pi(a_t|s_t) \triangleq p_\theta(\mathbf{x}_{T-t-1}|\mathbf{x}_{T-t}, \mathbf{c}), \quad (3)$$

$$r(s_t, a_t) \triangleq \begin{cases} R(\mathbf{x}_0, \mathbf{c}), & \text{if } t = T - 1 \\ 0, & \text{otherwise,} \end{cases} \quad (4)$$

where the denoising process p_θ parameterized by the diffusion model parameters θ is defined as the policy in this MDP. Starting with an initial state \mathbf{x}_T sampled from the noise distribution, at each step t , the policy treats the denoised sample \mathbf{x}_{T-t} as the current state s_t , and the next state \mathbf{x}_{T-t-1} as the action a_t . Trajectory rewards are defined sparsely, with only the final image \mathbf{x}_0 being evaluated using the predefined reward function $R(\mathbf{x}_0, \mathbf{c})$. Then the RL objective for diffusion models is to find the optimal diffusion policy that maximizes the expected reward of final images for prompts sampled from a distribution $p(\mathbf{c})$, i.e.,

$$\min_{\theta} \mathbb{E}_{p(\mathbf{c})} \mathbb{E}_{p_\theta(\mathbf{x}_0|\mathbf{c})} [-R(\mathbf{x}_0, \mathbf{c})]. \quad (5)$$

Optimization via policy gradient. Framing the denoising process as a diffusion policy enables exact computation of log-likelihoods and their gradients w.r.t. the diffusion model parameters θ . Given a full denoising trajectory $\mathbf{x}_{0:T}$, we can specifically compute the log-likelihood $\log p_\theta(\mathbf{x}_{t-1}|\mathbf{x}_t, \mathbf{c})$ for each denoising step. This allows for the computation of the log-likelihood gradient $\nabla_\theta \log p_\theta(\mathbf{x}_{t-1}|\mathbf{x}_t, \mathbf{c})$, which captures the sensitivity of each transition probability to changes in the model parameters. By exploiting this property, prior works such as DPOK [8] and DDPO [1] apply policy gradient methods [44, 50] to estimate the gradients of Eq. (5) as follows:

$$\mathbb{E}_{p(\mathbf{c})} \mathbb{E}_{p_\theta(\mathbf{x}_{0:T}|\mathbf{c})} \left[-R(\mathbf{x}_0, \mathbf{c}) \sum_{t=1}^T \nabla_\theta \log p_\theta(\mathbf{x}_{t-1}|\mathbf{x}_t, \mathbf{c}) \right]. \quad (6)$$

Reward difference learning. Inspired by direct preference optimization (DPO) [38] that converts the RL objective for language models into a supervised classification objective, recent approaches [5, 9] further derive a mean squared error-based objective for diffusion models, where the goal is to match the differences in log-likelihood ratios with the differences in rewards across paired denoising trajectories:

$$\mathbb{E}_{\mathbf{x}^a, \mathbf{x}^b, \mathbf{c}} \left[\sum_{t=1}^T \left(\frac{1}{\eta} \left(\log \frac{p_\theta(\mathbf{x}_t^a|\mathbf{c})}{p_{\theta'}(\mathbf{x}_t^a|\mathbf{c})} - \log \frac{p_\theta(\mathbf{x}_t^b|\mathbf{c})}{p_{\theta'}(\mathbf{x}_t^b|\mathbf{c})} \right) - (R(\mathbf{x}_0^a, \mathbf{c}) - R(\mathbf{x}_0^b, \mathbf{c})) \right)^2 \right]. \quad (7)$$

Here, \mathbf{x}_t^a and \mathbf{x}_t^b represent paired samples from the denoising step t of two independent trajectories, both generated using the same text prompt \mathbf{c} . These paired samples are used to compute the differences in their corresponding rewards, i.e. $R(\mathbf{x}_0^a, \mathbf{c}) - R(\mathbf{x}_0^b, \mathbf{c})$, as well as the differences in their log-likelihood ratios. In particular, $\log \frac{p_\theta(\mathbf{x}_t^a|\mathbf{c})}{p_{\theta'}(\mathbf{x}_t^a|\mathbf{c})}$ denotes the log-likelihood ratio of sample \mathbf{x}_t^a under the current model parameters θ compared to the previous or reference model parameters θ' , helping to quantify the change in the

model during online optimization. Furthermore, the *log-ratio scale factor* η is introduced to balance the contribution of log-ratio differences relative to reward differences in the objective, ensuring that neither term dominates the learning process. Empirically, both Deng *et al.* [5] and Gao *et al.* [9] demonstrate that this reward difference-based approach results in more stable reward optimization for diffusion models, compared to vanilla policy gradient methods [1, 8].

3. Method

3.1. Rethinking RL-based Finetuning of Few-Step Diffusion Models

To achieve RL-based finetuning of few-step diffusion models, we first consider three intuitive strategies:

- *The first strategy* involves training on short denoising trajectories (e.g. 1 or 2 steps). While it aligns with the few-step objective, this approach often leads to training instability and sample inefficiency, as detailed in Appendix B.
- *The second strategy* adopts the standard step settings (e.g. 50 steps) from prior works [1, 8], enabling more comprehensive learning. However, this approach risks overfitting to specific trajectory lengths, thereby compromising the model’s ability to generalize during inference with fewer steps, as shown in our experimental results in Sec. 4.2.
- *The third strategy* employs trajectories of varying lengths, which introduces diversity and may improve step generalization. However, the increased variance across trajectories can also lead to instability during training.

To improve step generalization while maintaining training stability, we propose to incorporate dense reward feedback throughout the entire denoising trajectory, rather than focusing solely on the sparse, final-step rewards. As introduced earlier in Sec. 2.1, the predicted original sample $\hat{\mathbf{x}}_t$ serves as the model’s intermediate estimate of the final, noise-free data at the corresponding denoising step t . In few-step diffusion models, the accuracy of the predicted $\hat{\mathbf{x}}_t$ at each denoising step t improves significantly, allowing even early iterations of $\hat{\mathbf{x}}_t$ to be used as reasonable approximations of the final generated sample. Remarkably, advanced few-step models such as SDXL-Turbo [42] enable high-quality single-step sampling, where the first prediction $\hat{\mathbf{x}}_{T-1}$ can already serve as a plausible generated output, with subsequent steps progressively refining the sample.

Dense feedback from $\hat{\mathbf{x}}^t$. Accordingly, we can utilize the predicted $\hat{\mathbf{x}}^t$ from each intermediate denoising step t to provide a dense, stepwise reward feedback. To achieve this, we refine the denoising MDP definition from Sec. 2.2 by applying the predefined reward function to each predicted $\hat{\mathbf{x}}_t$, yielding the updated formulation of Eq. (4) as follows:

$$r(s_t, a_t) \triangleq R(\hat{\mathbf{x}}_t, \mathbf{c}), \quad (8)$$

where each predicted $\hat{\mathbf{x}}_t$ can serve as a surrogate for the fi-

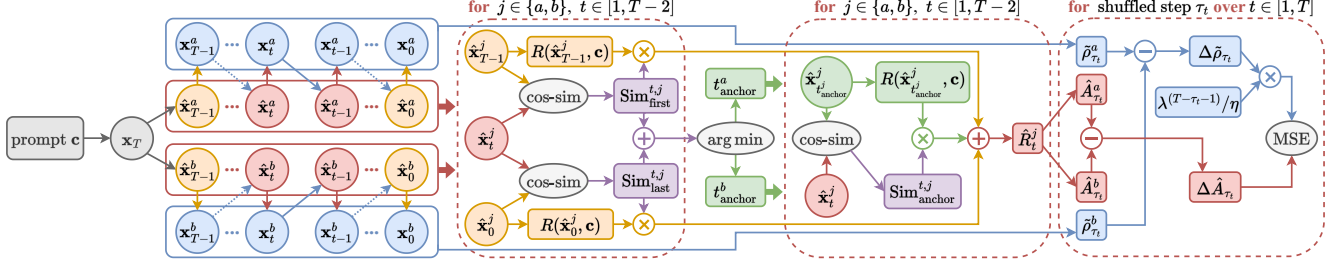


Figure 2. SDPO framework. SDPO begins by sampling two *denoised trajectories*, $\{\hat{\mathbf{x}}_{T-1}^a, \hat{\mathbf{x}}_{T-1}^b, \dots, \hat{\mathbf{x}}_0^a, \hat{\mathbf{x}}_0^b\}$, for reward estimation, alongside two corresponding *noisy trajectories*, $\{\mathbf{x}_{T-1}^a, \mathbf{x}_{T-1}^b, \dots, \mathbf{x}_0^a, \mathbf{x}_0^b\}$, for computing the *log-ratio* $\hat{\rho}_t$, using a shared *prompt* c and *initial noise* \mathbf{x}_T . For each denoised trajectory, the *reward function* R is queried only at the *first* ($t = T - 1$), *final* ($t = 0$), and an *anchor step* (t_{anchor}) adaptively selected based on cosine similarity. Additionally, cosine similarity is also applied to interpolate the *dense reward* \hat{R}_t for each step of the trajectories, informing the *advantage estimate* \hat{A}_t . Finally, for each *shuffled step* τ_t , we compute the MSE loss between the *advantage difference* $\Delta \hat{A}_{\tau_t}$ and the *log-ratio difference* $\Delta \hat{\rho}_{\tau_t}$, weighted by $\lambda^{(T-\tau_t-1)}/\eta$, thus enabling stepwise policy updates.

nal output of a full t -step denoising process. This dense reward feedback facilitates policy optimization at each intermediate step, introducing diversity into training with a fixed trajectory. Although variance still exists in different steps, it can be easily managed through reward normalization due to the consistency across trajectories. Ultimately, this stepwise optimization guides the model to progressively refine intermediate samples via dense rewards, striking a balance between generalization and stability in RL finetuning.

3.2. Dense Reward Difference Learning for Few-Step Diffusion Models

In this section, we present our approach to dense reward difference learning for few-step diffusion models. While dense rewards provide continuous feedback throughout the denoising process, directly querying rewards at each intermediate step is computationally intensive, as it requires decoding intermediate predictions $\hat{\mathbf{x}}_t$ from latent space to image space. To address this, we propose an efficient dense reward prediction method that leverages latent similarity, reducing reward queries while maintaining robust and granular guidance throughout the denoising process.

Dense reward prediction via latent similarity. Rather than querying rewards at every denoising step, we limit reward queries to three per trajectory: two fixed queries at the first and last steps, and one query at an adaptively selected intermediate step, referred to as the *anchor step*. To determine the anchor step, we first need to calculate the cosine similarity between the latent representations of each intermediate $\hat{\mathbf{x}}_t$ and those at the first and last steps, respectively:

$$\text{Sim}_{\text{first}}^t = \frac{\langle \hat{\mathbf{x}}_t, \hat{\mathbf{x}}_{T-1} \rangle}{\|\hat{\mathbf{x}}_t\| \|\hat{\mathbf{x}}_{T-1}\|}, \quad \text{Sim}_{\text{last}}^t = \frac{\langle \hat{\mathbf{x}}_t, \hat{\mathbf{x}}_0 \rangle}{\|\hat{\mathbf{x}}_t\| \|\hat{\mathbf{x}}_0\|}. \quad (9)$$

Then, the intermediate step that minimizes the sum of cosine similarities to the first and last steps is selected as the anchor step t_{anchor} , as it represents the step with the highest

divergence from the two extremes of the trajectory:

$$t_{\text{anchor}} = \arg \min_{t \in \{1, \dots, T-2\}} (\text{Sim}_{\text{first}}^t + \text{Sim}_{\text{last}}^t). \quad (10)$$

Once the anchor step t_{anchor} is identified, we further compute the cosine similarity between each intermediate step and the anchor step. This results in three cosine similarity values for each intermediate step t : (1) similarity to the first step, $\text{Sim}_{\text{first}}^t$, (2) similarity to the anchor step, $\text{Sim}_{\text{anchor}}^t$, and (3) similarity to the last step, $\text{Sim}_{\text{last}}^t$. These three similarity values are then used to perform a weighted averaging of the three reward queries, i.e., $R(\hat{\mathbf{x}}_{T-1}, c)$, $R(\hat{\mathbf{x}}_{t_{\text{anchor}}}, c)$, and $R(\hat{\mathbf{x}}_0, c)$ (abbr. R_{T-1} , $R_{t_{\text{anchor}}}$, and R_0), yielding an efficient estimation of each dense reward \hat{R}_t , as shown below:

$$\hat{R}_t = \frac{R_{T-1} \cdot \text{Sim}_{\text{first}}^t + R_{t_{\text{anchor}}} \cdot \text{Sim}_{\text{anchor}}^t + R_0 \cdot \text{Sim}_{\text{last}}^t}{\text{Sim}_{\text{first}}^t + \text{Sim}_{\text{anchor}}^t + \text{Sim}_{\text{last}}^t} \quad (11)$$

Dense reward difference learning. Leveraging this dense reward prediction method, we can now refine the reward difference learning approach, introduced in Sec. 2.2, into a more granular manner. Specifically, the objective is to match the difference in log-likelihood ratios, $\rho_t^j(\theta) := \log(p_\theta(\mathbf{x}_t^j | c) / p_{\theta'}(\mathbf{x}_t^j | c))$, with the difference in dense rewards \hat{R}_t^j at each step t for the paired trajectories $j \in \{a, b\}$:

$$\mathbb{E}_{\mathbf{x}_t^a, \mathbf{x}_t^b, c} \left[\left(\frac{1}{\eta} (\rho_t^a(\theta) - \rho_t^b(\theta)) - (\hat{R}_t^a - \hat{R}_t^b) \right)^2 \right]. \quad (12)$$

In contrast to the trajectory-level objective in Eq. (7), this stepwise objective enables more frequent model updates by eliminating the need to accumulate full trajectory data, thereby significantly improving sample efficiency.

3.3. Stepwise Diffusion Policy Optimization

In this section, we present Stepwise Diffusion Policy Optimization (SDPO), an online RL algorithm tailored for

stable, efficient optimization with dense reward difference learning. Building on our established studies from Secs. 3.1 and 3.2, SDPO introduces several key innovations that effectively exploit the stepwise granularity of our dense reward predictions, further enhancing sample efficiency and step generalization in finetuning few-step diffusion models.

To effectively facilitate optimization in a stepwise manner, it is crucial to incorporate feedback from other steps into the evaluation of the current step. In the online RL paradigm, although the log-likelihood ratios for other steps cannot be directly computed during each iteration of stepwise optimization, the dense rewards for the full trajectory are available from the sampling stage. Leveraging the availability of future feedback from dense rewards, SDPO calculates a cumulative return \hat{G}_t for each dense reward prediction \hat{R}_t with a *discount factor* $\gamma \in (0, 1]$, as shown below:

$$\hat{G}_t = \sum_{k=0}^t \gamma^k \hat{R}_{t-k}. \quad (13)$$

Per-step-prompt reward normalization. To reduce variance across different prompts, DDPO [1] applies a per-prompt normalization strategy, normalizing rewards by maintaining a running mean and standard deviation for each prompt individually. However, we aim to address not only the variance across prompts but also the variance across different denoising steps. Thus, we normalize the discounted return \hat{G}_t from Eq. (13) on a per-step-prompt basis, tracking running statistics independently for each step-prompt pair. This yields advantage estimates, \hat{A}_t^a and \hat{A}_t^b , at each step of both trajectories in Eq. (12), substituting \hat{R}_t^a and \hat{R}_t^b .

Stepwise importance weighting. Inspired by Yang *et al.* [24], we facilitate reward optimization for foundational image patterns in early denoising steps by applying stepwise importance weighting with a *decay rate* λ , to the log-likelihood ratios in our dense reward difference learning objective. Specifically, the stepwise importance weight follows an exponentially decaying pattern from the first step $t = T - 1$ to the last step $t = 0$, defined as $\lambda^{(T-t-1)}$. Thus, the objective becomes matching the log-ratio difference, $\Delta\rho_t(\theta) := \rho_t^a(\theta) - \rho_t^b(\theta)$, weighted by $\lambda^{(T-t-1)}/\eta$, with the corresponding advantage difference, $\Delta\hat{A}_t := \hat{A}_t^a - \hat{A}_t^b$, at each step t in paired trajectories:

$$l_\theta = \mathbb{E}_{\mathbf{x}_t^a, \mathbf{x}_t^b, \mathbf{c}} \left[\left(\Delta\rho_t(\theta) \cdot \lambda^{(T-t-1)}/\eta - \Delta\hat{A}_t \right)^2 \right] \quad (14)$$

Additionally, to prevent large, unstable policy updates during online optimization, we constrain the log-likelihood ratios within a trust region by clipping them at a threshold ϵ . Defining the clipped ratios as $\tilde{\rho}_t^j(\theta) := \text{clip}(\rho_t^j(\theta), -\epsilon, \epsilon)$, we can express the clipped objective as follows:

$$\tilde{l}_\theta = \mathbb{E}_{\mathbf{x}_t^a, \mathbf{x}_t^b, \mathbf{c}} \left[\left(\Delta\tilde{\rho}_t(\theta) \cdot \lambda^{(T-t-1)}/\eta - \Delta\hat{A}_t \right)^2 \right] \quad (15)$$

Algorithm 1 Stepwise Diffusion Policy Optimization

- 1: **Input:** Pretrained diffusion model p_θ , prompt distribution $p(\mathbf{c})$, number of training epochs E , number of denoising steps per trajectory T , batch size B
 - 2: **for** epoch $e = 1, \dots, E$ **do**
 - 3: Store the previous model $p_{\theta'} \leftarrow p_\theta$
 - 4: Sample prompts $\{\mathbf{c}_i \sim p(\mathbf{c})\}_{i=1}^B$
 - 5: Generate trajectories $\{(\mathbf{x}^{a,i}, \mathbf{x}^{b,i}) \sim p_{\theta'}(\mathbf{x}|\mathbf{c}_i)\}_{i=1}^B$
 - 6: **for** batch $i = 1, \dots, B$ **do**
 - 7: Compute rewards $\{\hat{R}_t^{a,i}, \hat{R}_t^{b,i}\}_{t=0}^{T-1}$ via Eq. (11)
 - 8: Compute returns $\{\hat{G}_t^{a,i}, \hat{G}_t^{b,i}\}_{t=0}^{T-1}$ via Eq. (13)
 - 9: Normalize returns per step-prompt pair, and get advantage estimates $\{\hat{A}_t^{a,i}, \hat{A}_t^{b,i}\}_{t=0}^{T-1}$
 - 10: Generate shuffled step indices $\{\tau_t^i\}_{t=0}^{T-1}$
 - 11: **end for**
 - 12: **for** step $t = 1, \dots, T$ **do**
 - 13: Update the current model p_θ via Eq. (16)
 - 14: **end for**
 - 15: **end for**
-

Step-shuffled gradient updates. To implement stepwise gradient updates for Eq. (14), SDPO incorporates a novel step-shuffled update strategy, where each gradient update selects data from a single step in each independently shuffled trajectory. In each training epoch, SDPO performs T updates, corresponding to the number of steps per trajectory, with training samples divided into B batches, each containing a pair of trajectories. To avoid overfitting to specific denoising steps, all trajectories are independently shuffled along the step dimension within each batch. Let τ_i represent the shuffled step indices for the i -th batch, then the t -th gradient update for θ is formulated as:

$$\mathcal{L}_t(\theta) \leftarrow \frac{1}{B} \sum_{i=1}^B \max \left(l_\theta(\mathbf{x}_{\tau_t^i}^{a,i}, \mathbf{x}_{\tau_t^i}^{b,i}, \mathbf{c}_i), \tilde{l}_\theta(\mathbf{x}_{\tau_t^i}^{a,i}, \mathbf{x}_{\tau_t^i}^{b,i}, \mathbf{c}_i) \right), \quad (16)$$

where we select the maximum value between the unclipped objective l_θ and the clipped objective \tilde{l}_θ , both calculated using samples $(\mathbf{x}_{\tau_t^i}^{a,i}, \mathbf{x}_{\tau_t^i}^{b,i}, \mathbf{c}_i)$ from the τ_t^i -th step of the paired trajectories in the i -th batch. The pseudo-code of SDPO is in Algorithm 1, with the overall framework shown in Fig. 2.

4. Experiments

In this section, we present comprehensive experiments to validate the efficacy of our SDPO in finetuning few-step diffusion models with various reward functions.

4.1. Experimental Setup

In our main experiments (Secs. 4.2 and 4.3), we use SD-Turbo [42], a few-step text-to-image model distilled from Stable Diffusion v2.1 [40] through adversarial diffusion dis-

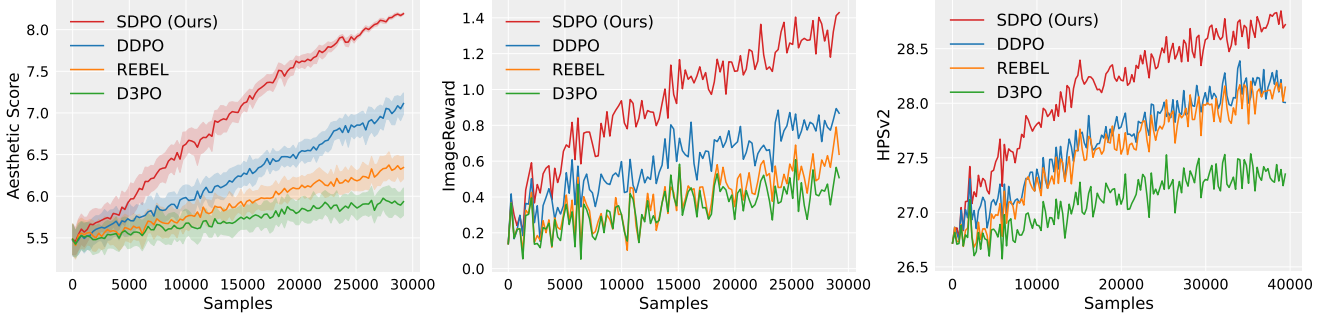


Figure 3. Learning curves by sample efficiency. Reward scores (left: Aesthetic Score, middle: ImageReward, right: HPSv2) are evaluated for images generated with 50 denoising steps. The horizontal axis represents the cumulative number of training samples.

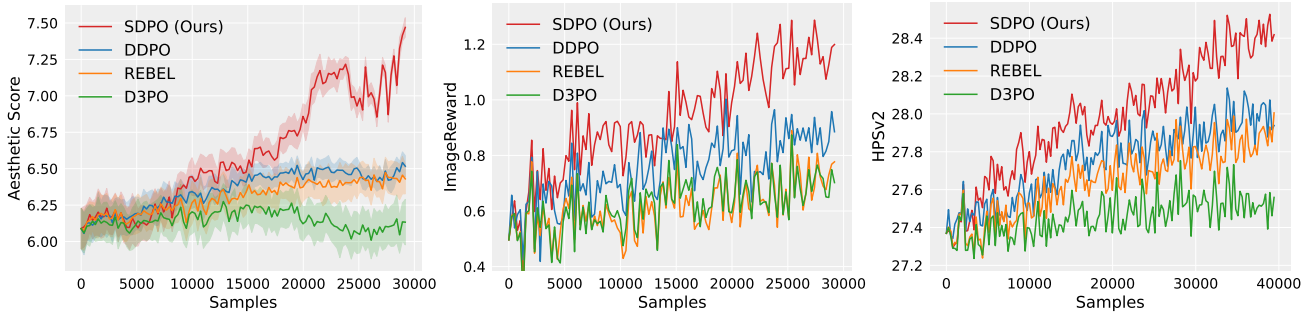


Figure 4. Evaluation curves for generalization to 1-step. Reward scores are evaluated for images generated with a single denoising step.

tillation [42], as the base model. For efficient finetuning, we apply Low-Rank Adaptation (LoRA) [14], which enables updating only the LoRA weights while freezing the pre-trained model parameters. Following DDPO [1], we generate denoising trajectories using the DDIM sampler [46] with 50 denoising steps and a prompt set of 45 animal names. Since SD-Turbo does not support classifier-free guidance or negative prompts, we disable them by setting the guidance scale to 1.0. The model is finetuned separately with four commonly used reward functions: Aesthetic Score [43], ImageReward [54], HPSv2 [51], and PickScore [17].

4.2. Algorithm Comparisons

We compare the reward optimization performance of SDPO with DDPO [1], REBEL [9], and D3PO [55], each exemplifying a distinct approach to diffusion alignment: policy gradient methods, reward difference-based methods, and DPO-style methods, respectively. As each of these methods was originally implemented for different diffusion model variations, we reconfigure them to operate consistently on SD-Turbo. For a fair comparison, we standardize key hyperparameters across all algorithms, such as denoising steps per trajectory ($T = 50$) and training samples per epoch.

Sample efficiency in reward optimization. We prioritize sample efficiency as a key metric for evaluating reward optimization performance, examining how effectively each algorithm utilizes generated samples to improve reward out-

comes. Learning curves in Fig. 3 illustrate the sample efficiency of each algorithm during reward optimization with 50-step denoising across different reward functions. The horizontal axis specifies the cumulative number of generated image samples utilized for reward optimization, while the vertical axis reflects the average reward values calculated from these samples. In Fig. 3, the steeper learning curves of SDPO suggest that our method is able to achieve higher reward scores with relatively fewer samples compared to others, indicating its superior sample efficiency.

Step generalization. We evaluate the step generalization capabilities of models finetuned on 50-step denoising trajectories during inference with fewer denoising steps, where samples are generated using varying number of denoising steps (1, 2, 4, 8, and 16). Specifically, we leverage each intermediate model checkpoint to generate samples with different step configurations, subsequently evaluating these samples across various reward functions. Figure 4 presents the reward curves for samples generated using a single denoising step, while additional curves for samples from denoising trajectories of other lengths are provided in Appendix E. Across all evaluations, our SDPO consistently achieves the highest reward scores compared to other algorithms, indicating superior step generalization.

Generalization to unseen prompts. We further evaluate finetuned models on unseen prompts from [8], which

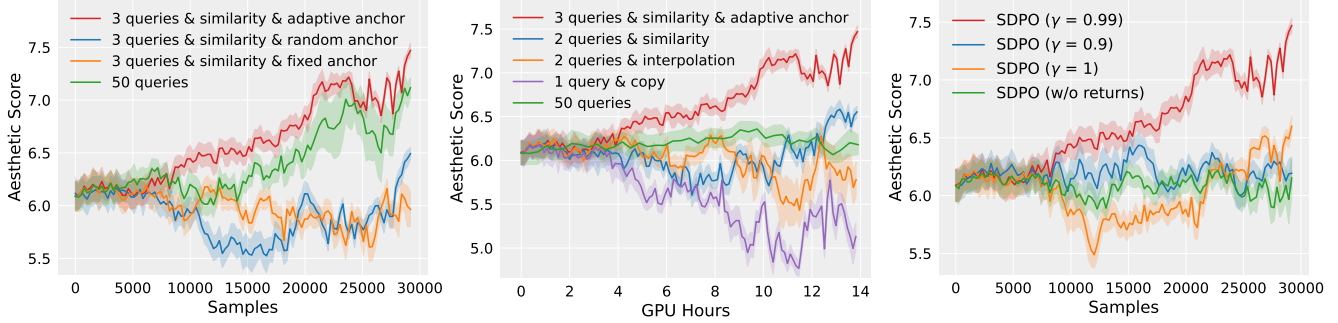


Figure 5. Ablation study on dense reward prediction (left & middle) and discounted returns (right) for SDPO.

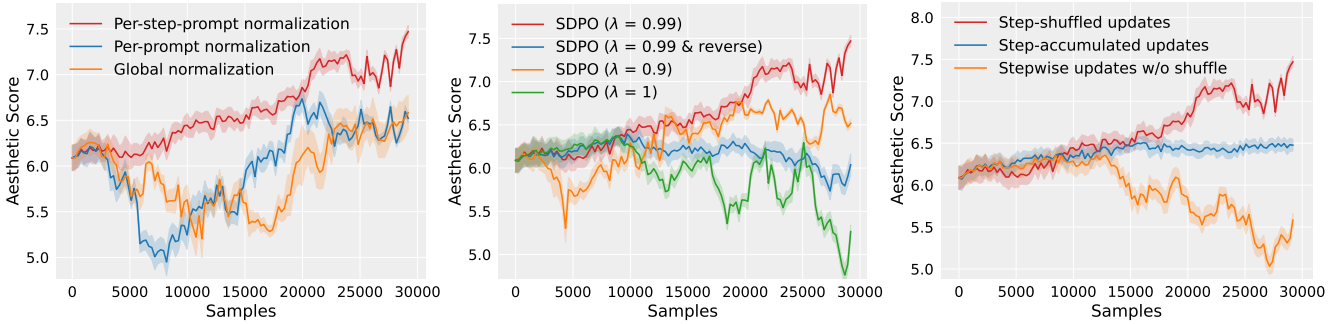


Figure 6. Ablation study on reward normalization (left), importance weighting (middle), and gradient updates (right) for SDPO.

specify attributes like color (*A green colored rabbit*), count (*Four wolves in the park*), composition (*A cat and a dog*), and location (*A dog on the moon*). Table 1 displays reward scores for sampling trajectories of 1, 4, 16, and 50 steps, evaluated using various reward functions. Across all these evaluations, our SDPO continues to outperform the pretrained SD-Turbo and the other algorithms. We also present qualitative comparisons of generated images for unseen prompts in Fig. 1 and Appendix F, where SDPO consistently delivers reward-aligned images across all steps.

4.3. Ablation Study

We conduct a series of ablation studies to systematically analyze the impact of each key component in our SDPO on its generalization performance to reward evaluations for 1-step sampling. Notably, we optimize Aesthetic Score in these studies, as it lacks supervision for text-image alignment, presenting a greater challenge for achieving generalization.

Effect of dense reward prediction. As detailed in Sec. 3.2, we use 3 reward queries per trajectory, latent similarity, and an adaptively selected anchor to efficiently predict dense rewards. To examine the effectiveness of this approach, we compare SDPO with variations that employ alternative strategies for dense reward prediction, including:

- *3 queries & similarity & adaptive anchor*: Original setup.
- *3 queries & similarity & random anchor*: In this variation, we still use 3 reward queries per trajectory and lever-

age latent similarity, but instead of selecting the anchor based on adaptive criteria, we select it purely at random.

- *3 queries & similarity & fixed anchor*: In this setup, we again use 3 reward queries and latent similarity but set a fixed anchor at the 25th step for all trajectories.
- *2 queries & similarity*: Here, we reduce the number of reward queries from 3 to 2, continuing to use latent similarity to guide predictions but without relying on an anchor.
- *2 queries & interpolation*: In this method, we also use 2 reward queries but replace latent similarity with an interpolation method to approximate intermediate rewards.
- *1 query & copy*: Here, a single reward query is used per trajectory and is copied across all denoising steps.
- *50 queries*: This variation greatly increases reward queries to 50 per trajectory, maximizing the reward density without the need for interpolation or similarity.

The left plot in Fig. 5 compares the generalization performance of SDPO variations, using 3 and 50 reward queries, by evaluating rewards from 1-step sampling during training. The middle plot in Fig. 5 evaluates the training time efficiency of different dense reward prediction methods, using GPU hours on the x-axis. Our proposed method consistently outperforms all the variations, demonstrating its effectiveness in predicting dense rewards. Notably, while the variation with 50 reward queries demonstrates comparable sample efficiency to the original method, it necessitates substantially more computational time. In contrast, our ap-

Table 1. Generalization to unseen prompts. *1s*, *4s*, *16s*, and *50s* indicate 1-step, 4-step, 16-step, and 50-step denoising, respectively.

Method	ImageReward				Aesthetic Score				HPSv2				PickScore			
	<i>1s</i>	<i>4s</i>	<i>16s</i>	<i>50s</i>	<i>1s</i>	<i>4s</i>	<i>16s</i>	<i>50s</i>	<i>1s</i>	<i>4s</i>	<i>16s</i>	<i>50s</i>	<i>1s</i>	<i>4s</i>	<i>16s</i>	<i>50s</i>
SD-Turbo [42]	0.985	0.927	1.063	0.392	6.049	5.920	5.820	5.432	27.83	27.96	28.34	27.40	22.60	22.65	22.70	21.78
D3PO [55]	1.152	1.009	1.196	0.801	6.285	6.167	6.102	5.958	28.06	28.21	28.65	28.19	22.59	22.65	22.79	22.36
DDPO [1]	1.191	1.084	1.155	1.088	6.610	6.619	6.604	6.733	28.48	28.50	28.59	28.73	22.53	22.64	22.87	22.81
REBEL [9]	1.139	1.128	1.189	0.918	6.487	6.411	6.329	6.245	28.33	28.38	28.70	28.79	22.48	22.54	22.74	22.73
SDPO (Ours)	1.609	1.576	1.556	1.573	7.077	7.333	7.802	8.175	28.77	28.87	29.23	29.26	22.80	22.94	23.46	23.86

proach not only achieves high sample efficiency but also significantly enhances computational efficiency, due to its superior effectiveness in addressing step generalization.

Effect of discounted returns. We then evaluate SDPO with different discount factors: $\gamma = 0.99, 0.9$, and 1 , along with a variation that directly uses rewards without returns. As shown in the right plot of Fig. 5, SDPO with $\gamma = 0.99$ achieves the best performance in step generalization.

Effect of per-step-prompt normalization. We also compare the per-step-prompt normalization strategy in SDPO with two alternatives: (1) *per-prompt normalization*, which normalizes rewards on a per prompt basis, and (2) *global normalization*, which simply normalizes rewards across all samples. The left plot in Fig. 6 shows both alternatives underperform our per-step-prompt normalization.

Effect of stepwise importance weighting. We further analyze the impact of stepwise importance weighting in SDPO with different decay factors: $\lambda = 0.99, 0.9$, and 1 , as well as a variation that applies weights in a *reverse* order. As shown in the middle plot of Fig. 6, SDPO with $\lambda = 0.99$ achieves the best step generalization performance.

Effect of step-shuffled gradient updates. Finally, we evaluate the impact of replacing step-shuffled updates in SDPO with two alternative strategies: (1) *step-accumulated updates* and (2) *stepwise updates without shuffling*. The right plot in Fig. 6 shows both alternatives underperform our step-shuffled updates. Step-accumulated updates, by accumulating gradients over all denoising steps, lead to a significant decay in sample efficiency. Meanwhile, stepwise updates without shuffling demonstrate poor step generalization, likely due to overfitting to the fixed step order.

4.4. Extension to Consistency Models

We further explore finetuning consistency models with our SDPO by utilizing the RLCM baseline [34], which applies both DDPO and REBEL for finetuning a latent consistency model [28] distilled from Dreamshaper v7 [30]. As shown in Figure 12, SDPO still outperforms DDPO and REBEL in reward optimization for the latent consistency model.

5. Related Work

Diffusion model alignment. Existing approaches for diffusion alignment [18, 26, 52] can be broadly classified into

two categories: (1) reward-based methods, which use techniques such as policy gradient-based RL finetuning [1, 2, 8, 11, 19, 32, 48, 60, 61], reward difference [5, 9], or reward backpropagation through sampling [3, 22, 36, 37, 53] to optimize the model based on explicit reward functions; and (2) preference-based methods [4, 10, 13, 15, 21, 24, 49, 55, 56, 59], which employ DPO-style objectives to directly align the model with data-driven preferences. Our work is motivated by the reward difference methods. Despite their efficacy in aligning multi-step diffusion models, they often fail in direct applications to few-step diffusion models.

Alignment of few-step diffusion models. Recent approaches [20, 39] incorporate reward guidance into consistency distillation, while not directly applicable to other distilled few-step models. RLCM [34] introduces an RL finetuning framework specifically for consistency models, which we use as a baseline in our extensive analysis of applying our SDPO to consistency models. In contrast, our work extends RL finetuning to arbitrary few-step diffusion models, while addressing the step generalization problem.

Dense feedback for diffusion models. Recent studies have explored dense feedback in diffusion alignment. For RL finetuning, Zhang *et al.* [61] highlight the importance of dense rewards to prevent overoptimization, and introduce a temporal critic to estimate dense rewards. For preference learning, Yang *et al.* [56] apply temporal discounting in a DPO-style objective to distinguish preferences at each step, while Liang *et al.* [24] build a step-aware preference model to provide stepwise preference. In contrast, our work incorporates dense rewards into RL finetuning of few-step diffusion models without requiring additional model training.

6. Conclusion

This paper presented SDPO, an RL framework that aligns few-step diffusion models with downstream objectives via dense reward difference learning. By leveraging our dense reward predictions alongside novel strategies designed to exploit their stepwise granularity, SDPO effectively addresses the step generalization problem. Our experiments demonstrate that SDPO achieves robust diffusion alignment across diverse step configurations, showcasing its potential for practical applications of few-step diffusion models.

References

- [1] Kevin Black, Michael Janner, Yilun Du, Ilya Kostrikov, and Sergey Levine. Training diffusion models with reinforcement learning. In *International Conference on Learning Representations*, 2024. 1, 2, 3, 5, 6, 8, 12, 13
- [2] Chaofeng Chen, Annan Wang, Haoning Wu, Liang Liao, Wenxiu Sun, Qiong Yan, and Weisi Lin. Enhancing diffusion models with text-encoder reinforcement learning. In *European Conference on Computer Vision*, pages 182–198, 2024. 8
- [3] Kevin Clark, Paul Vicol, Kevin Swersky, and David J Fleet. Directly fine-tuning diffusion models on differentiable rewards. In *International Conference on Learning Representations*, 2024. 8
- [4] Florinel-Alin Croitoru, Vlad Hondru, Radu Tudor Ionescu, Nicu Sebe, and Mubarak Shah. Curriculum direct preference optimization for diffusion and consistency models. *arXiv preprint arXiv:2405.13637*, 2024. 8
- [5] Fei Deng, Qifei Wang, Wei Wei, Tingbo Hou, and Matthias Grundmann. PRDP: Proximal reward difference prediction for large-scale reward finetuning of diffusion models. In *Proceedings of the IEEE/CVF Conference on Computer Vision and Pattern Recognition*, pages 7423–7433, 2024. 2, 3, 8
- [6] Patrick Esser, Sumith Kulal, Andreas Blattmann, Rahim Entezari, Jonas Müller, Harry Saini, Yam Levi, Dominik Lorenz, Axel Sauer, Frederic Boesel, Dustin Podell, Tim Dockhorn, Zion English, and Robin Rombach. Scaling rectified flow transformers for high-resolution image synthesis. In *International Conference on Machine Learning*, pages 12606–12633, 2024. 1
- [7] Ying Fan and Kangwook Lee. Optimizing DDPM sampling with shortcut fine-tuning. In *International Conference on Machine Learning*, pages 9623–9639, 2023. 2
- [8] Ying Fan, Olivia Watkins, Yuqing Du, Hao Liu, Moonkyung Ryu, Craig Boutilier, Pieter Abbeel, Mohammad Ghavamzadeh, Kangwook Lee, and Kimin Lee. DPOK: Reinforcement learning for fine-tuning text-to-image diffusion models. *Advances in Neural Information Processing Systems*, 36:79858–79885, 2023. 2, 3, 6, 8
- [9] Zhaolin Gao, Jonathan D Chang, Wenhao Zhan, Owen Oertell, Gokul Swamy, Kianté Brantley, Thorsten Joachims, J Andrew Bagnell, Jason D Lee, and Wen Sun. REBEL: Reinforcement learning via regressing relative rewards. *arXiv preprint arXiv:2404.16767*, 2024. 2, 3, 6, 8, 12, 13
- [10] Yi Gu, Zhendong Wang, Yueqin Yin, Yujia Xie, and Mingyuan Zhou. Diffusion-rpo: Aligning diffusion models through relative preference optimization. *arXiv preprint arXiv:2406.06382*, 2024. 8
- [11] Yaru Hao, Zewen Chi, Li Dong, and Furu Wei. Optimizing prompts for text-to-image generation. *Advances in Neural Information Processing Systems*, 36:66923–66939, 2023. 8
- [12] Jonathan Ho, Ajay Jain, and Pieter Abbeel. Denoising diffusion probabilistic models. *Advances in Neural Information Processing Systems*, 33:6840–6851, 2020. 2
- [13] Jiwoo Hong, Sayak Paul, Noah Lee, Kashif Rasul, James Thorne, and Jongheon Jeong. Margin-aware preference optimization for aligning diffusion models without reference. *arXiv preprint arXiv:2406.06424*, 2024. 8
- [14] Edward J Hu, Yelong Shen, Phillip Wallis, Zeyuan Allen-Zhu, Yuanzhi Li, Shean Wang, Lu Wang, and Weizhu Chen. LoRA: Low-rank adaptation of large language models. In *International Conference on Learning Representations*, 2022. 6
- [15] Shyamgopal Karthik, Huseyin Coskun, Zeynep Akata, Sergey Tulyakov, Jian Ren, and Anil Kag. Scalable ranked preference optimization for text-to-image generation. *arXiv preprint arXiv:2410.18013*, 2024. 8
- [16] Dongjun Kim, Chieh-Hsin Lai, Wei-Hsiang Liao, Naoki Murata, Yuhta Takida, Toshimitsu Uesaka, Yutong He, Yuki Mitsufuji, and Stefano Ermon. Consistency trajectory models: Learning probability flow ODE trajectory of diffusion. In *The Twelfth International Conference on Learning Representations*, 2024. 1
- [17] Yuval Kirstain, Adam Polyak, Uriel Singer, Shahbuland Matiana, Joe Penna, and Omer Levy. Pick-a-pic: An open dataset of user preferences for text-to-image generation. *Advances in Neural Information Processing Systems*, 36:36652–36663, 2023. 1, 2, 6, 14
- [18] Kimin Lee, Hao Liu, Moonkyung Ryu, Olivia Watkins, Yuqing Du, Craig Boutilier, Pieter Abbeel, Mohammad Ghavamzadeh, and Shixiang Shane Gu. Aligning text-to-image models using human feedback. *arXiv preprint arXiv:2302.12192*, 2023. 8
- [19] Seung Hyun Lee, Yinxiao Li, Junjie Ke, Innfarn Yoo, Han Zhang, Jiahui Yu, Qifei Wang, Fei Deng, Glenn Entis, Junfeng He, et al. Parrot: Pareto-optimal multi-reward reinforcement learning framework for text-to-image generation. In *European Conference on Computer Vision*, pages 462–478, 2025. 8
- [20] Jiachen Li, Weixi Feng, Wenhao Chen, and William Yang Wang. Reward guided latent consistency distillation. *Transactions on Machine Learning Research*, 2024. 8
- [21] Shufan Li, Konstantinos Kallidromitis, Akash Gokul, Yusuke Kato, and Kazuki Kozuka. Aligning diffusion models by optimizing human utility. *arXiv preprint arXiv:2404.04465*, 2024. 8
- [22] Yanyu Li, Xian Liu, Anil Kag, Ju Hu, Yerlan Idelbayev, Dhritiman Sagar, Yanzhi Wang, Sergey Tulyakov, and Jian Ren. Textcrafter: Your text encoder can be image quality controller. In *Proceedings of the IEEE/CVF Conference on Computer Vision and Pattern Recognition*, pages 7985–7995, 2024. 8
- [23] Youwei Liang, Junfeng He, Gang Li, Peizhao Li, Arseniy Klimovskiy, Nicholas Carolan, Jiao Sun, Jordi Pont-Tuset, Sarah Young, Feng Yang, Junjie Ke, Krishnamurthy Dj Dvijotham, Katherine M. Collins, Yiwen Luo, Yang Li, Kai J Kohlhoff, Deepak Ramachandran, and Vidhya Navalpakkam. Rich human feedback for text-to-image generation. In *Proceedings of the IEEE/CVF Conference on Computer Vision and Pattern Recognition*, pages 19401–19411, 2024. 2
- [24] Zhanhao Liang, Yuhui Yuan, Shuyang Gu, Bohan Chen, Tiankai Hang, Ji Li, and Liang Zheng. Step-aware prefer-

- ence optimization: Aligning preference with denoising performance at each step. *arXiv preprint arXiv:2406.04314*, 2024. 5, 8
- [25] Shanchuan Lin, Anran Wang, and Xiao Yang. Sdxl-lightning: Progressive adversarial diffusion distillation. *arXiv preprint arXiv:2402.13929*, 2024. 1
- [26] Buhua Liu, Shitong Shao, Bao Li, Lichen Bai, Haoyi Xiong, James Kwok, Sumi Helal, and Zeke Xie. Alignment of diffusion models: Fundamentals, challenges, and future. *arXiv preprint arXiv:2409.07253*, 2024. 8
- [27] Xingchao Liu, Xiwen Zhang, Jianzhu Ma, Jian Peng, and Qiang Liu. Instaflo: One step is enough for high-quality diffusion-based text-to-image generation. In *International Conference on Learning Representations*, 2024. 1
- [28] Simian Luo, Yiqin Tan, Longbo Huang, Jian Li, and Hang Zhao. Latent Consistency Models: Synthesizing high-resolution images with few-step inference. *arXiv preprint arXiv:2310.04378*, 2023. 8, 13
- [29] Weijian Luo, Tianyang Hu, Shifeng Zhang, Jiacheng Sun, Zhenguo Li, and Zhihua Zhang. Diff-Instruct: A universal approach for transferring knowledge from pre-trained diffusion models. *Advances in Neural Information Processing Systems*, 36:76525–76546, 2023. 1
- [30] Lykon. Dreamshaper v7. <https://huggingface.co/Lykon/dreamshaper-7>, 2023. 8
- [31] Chenlin Meng, Robin Rombach, Ruiqi Gao, Diederik Kingma, Stefano Ermon, Jonathan Ho, and Tim Salimans. On distillation of guided diffusion models. In *Proceedings of the IEEE/CVF Conference on Computer Vision and Pattern Recognition*, pages 14297–14306, 2023. 1
- [32] Wenyi Mo, Tianyu Zhang, Yalong Bai, Bing Su, Ji-Rong Wen, and Qing Yang. Dynamic prompt optimizing for text-to-image generation. In *Proceedings of the IEEE/CVF Conference on Computer Vision and Pattern Recognition*, pages 26627–26636, 2024. 8
- [33] Thuan Hoang Nguyen and Anh Tran. SwiftBrush: One-step text-to-image diffusion model with variational score distillation. In *Proceedings of the IEEE/CVF Conference on Computer Vision and Pattern Recognition*, pages 7807–7816, 2024. 1
- [34] Owen Oertell, Jonathan Daniel Chang, Yiyi Zhang, Kianté Brantley, and Wen Sun. RL for consistency models: Reward guided text-to-image generation with fast inference. *Reinforcement Learning Journal*, 4:1656–1673, 2024. 8, 13
- [35] Dustin Podell, Zion English, Kyle Lacey, Andreas Blattmann, Tim Dockhorn, Jonas Müller, Joe Penna, and Robin Rombach. SDXL: Improving latent diffusion models for high-resolution image synthesis. In *International Conference on Learning Representations*, 2024. 1
- [36] Mihir Prabhudesai, Anirudh Goyal, Deepak Pathak, and Katerina Fragkiadaki. Aligning text-to-image diffusion models with reward backpropagation. *arXiv preprint arXiv:2310.03739*, 2023. 8
- [37] Mihir Prabhudesai, Russell Mendonca, Zheyang Qin, Katerina Fragkiadaki, and Deepak Pathak. Video diffusion alignment via reward gradients. *arXiv preprint arXiv:2407.08737*, 2024. 8
- [38] Rafael Rafailov, Archit Sharma, Eric Mitchell, Christopher D Manning, Stefano Ermon, and Chelsea Finn. Direct preference optimization: Your language model is secretly a reward model. *Advances in Neural Information Processing Systems*, 36:53728–53741, 2023. 3
- [39] Yuxi Ren, Xin Xia, Yanzuo Lu, Jiacheng Zhang, Jie Wu, Pan Xie, Xing Wang, and Xuefeng Xiao. Hyper-sd: Trajectory segmented consistency model for efficient image synthesis. *arXiv preprint arXiv:2404.13686*, 2024. 8
- [40] Robin Rombach, Andreas Blattmann, Dominik Lorenz, Patrick Esser, and Björn Ommer. High-resolution image synthesis with latent diffusion models. In *Proceedings of the IEEE/CVF Conference on Computer Vision and Pattern Recognition*, pages 10684–10695, 2022. 1, 5
- [41] Tim Salimans and Jonathan Ho. Progressive distillation for fast sampling of diffusion models. In *International Conference on Learning Representations*, 2022. 1
- [42] Axel Sauer, Dominik Lorenz, Andreas Blattmann, and Robin Rombach. Adversarial diffusion distillation. *arXiv preprint arXiv:2311.17042*, 2023. 1, 3, 5, 6, 8, 12, 13
- [43] Christoph Schuhmann, Romain Beaumont, Richard Vencu, Cade W Gordon, Ross Wightman, Mehdi Cherti, Theo Coombes, Aarush Katta, Clayton Mullis, Mitchell Wortsman, Patrick Schramowski, Srivatsa R Kundurthy, Katherine Crowson, Ludwig Schmidt, Robert Kaczmarczyk, and Jenia Jitsev. LAION-5B: An open large-scale dataset for training next generation image-text models. *Advances in Neural Information Processing Systems*, 35:25278–25294, 2022. 2, 6, 14
- [44] John Schulman, Filip Wolski, Prafulla Dhariwal, Alec Radford, and Oleg Klimov. Proximal policy optimization algorithms. *arXiv preprint arXiv:1707.06347*, 2017. 3
- [45] Jascha Sohl-Dickstein, Eric Weiss, Niru Maheswaranathan, and Surya Ganguli. Deep unsupervised learning using nonequilibrium thermodynamics. In *International Conference on Machine Learning*, pages 2256–2265, 2015. 1
- [46] Jiaming Song, Chenlin Meng, and Stefano Ermon. Denoising diffusion implicit models. In *International Conference on Learning Representations*, 2021. 6
- [47] Yang Song, Prafulla Dhariwal, Mark Chen, and Ilya Sutskever. Consistency models. In *International Conference on Machine Learning*, pages 32211–32252, 2023. 1, 12
- [48] Masatoshi Uehara, Yulai Zhao, Kevin Black, Ehsan Hajiramezanali, Gabriele Scalia, Nathaniel Lee Diamant, Alex M Tseng, Sergey Levine, and Tommaso Biancalani. Feedback efficient online fine-tuning of diffusion models. In *International Conference on Machine Learning*, pages 48892–48918, 2024. 8
- [49] Bram Wallace, Meihua Dang, Rafael Rafailov, Linqi Zhou, Aaron Lou, Senthil Purushwalkam, Stefano Ermon, Caiming Xiong, Shafiq Joty, and Nikhil Naik. Diffusion model alignment using direct preference optimization. In *Proceedings of the IEEE/CVF Conference on Computer Vision and Pattern Recognition*, pages 8228–8238, 2024. 8
- [50] Ronald J Williams. Simple statistical gradient-following algorithms for connectionist reinforcement learning. *Machine learning*, 8:229–256, 1992. 3

- [51] Xiaoshi Wu, Yiming Hao, Keqiang Sun, Yixiong Chen, Feng Zhu, Rui Zhao, and Hongsheng Li. Human Preference Score v2: A solid benchmark for evaluating human preferences of text-to-image synthesis. *arXiv preprint arXiv:2306.09341*, 2023. [2](#), [6](#), [14](#)
- [52] Xiaoshi Wu, Keqiang Sun, Feng Zhu, Rui Zhao, and Hongsheng Li. Human Preference Score: Better aligning text-to-image models with human preference. In *Proceedings of the IEEE/CVF International Conference on Computer Vision*, pages 2096–2105, 2023. [8](#)
- [53] Xiaoshi Wu, Yiming Hao, Manyuan Zhang, Keqiang Sun, Zhaoyang Huang, Guanglu Song, Yu Liu, and Hongsheng Li. Deep reward supervisions for tuning text-to-image diffusion models. *arXiv preprint arXiv:2405.00760*, 2024. [8](#)
- [54] Jiazheng Xu, Xiao Liu, Yuchen Wu, Yuxuan Tong, Qinkai Li, Ming Ding, Jie Tang, and Yuxiao Dong. ImageReward: Learning and evaluating human preferences for text-to-image generation. *Advances in Neural Information Processing Systems*, 36:15903–15935, 2023. [2](#), [6](#), [14](#)
- [55] Kai Yang, Jian Tao, Jiafei Lyu, Chunjiang Ge, Jiabin Chen, Weihai Shen, Xiaolong Zhu, and Xiu Li. Using human feedback to fine-tune diffusion models without any reward model. In *Proceedings of the IEEE/CVF Conference on Computer Vision and Pattern Recognition*, pages 8941–8951, 2024. [6](#), [8](#), [12](#), [13](#)
- [56] Shentao Yang, Tianqi Chen, and Mingyuan Zhou. A dense reward view on aligning text-to-image diffusion with preference. In *International Conference on Machine Learning*, pages 55998–56032, 2024. [8](#)
- [57] Tianwei Yin, Michaël Gharbi, Taesung Park, Richard Zhang, Eli Shechtman, Fredo Durand, and William T. Freeman. Improved distribution matching distillation for fast image synthesis. *Advances in Neural Information Processing Systems*, 37, 2024. [1](#)
- [58] Tianwei Yin, Michaël Gharbi, Richard Zhang, Eli Shechtman, Frédo Durand, William T. Freeman, and Taesung Park. One-step diffusion with distribution matching distillation. In *Proceedings of the IEEE/CVF Conference on Computer Vision and Pattern Recognition*, pages 6613–6623, 2024. [1](#)
- [59] Huizhuo Yuan, Zixiang Chen, Kaixuan Ji, and Quanquan Gu. Self-play fine-tuning of diffusion models for text-to-image generation. *arXiv preprint arXiv:2402.10210*, 2024. [8](#)
- [60] Yinan Zhang, Eric Tzeng, Yilun Du, and Dmitry Kislyuk. Large-scale reinforcement learning for diffusion models. *arXiv preprint arXiv:2401.12244*, 4, 2024. [8](#)
- [61] Ziyi Zhang, Sen Zhang, Yibing Zhan, Yong Luo, Yonggang Wen, and Dacheng Tao. Confronting reward overoptimization for diffusion models: A perspective of inductive and primacy biases. In *International Conference on Machine Learning*, pages 60396–60413, 2024. [8](#)

A. Implementation Details

A.1. Main Experimental Setup

For our main experiments in Sec. 4.2, we use SD-Turbo [42] as the base model to compare the performance of DDPO [1], REBEL [9], D3PO [55], and our proposed SDPO in finetuning few-step diffusion models. Detailed implementation for each of these methods is provided below:

DDPO implementation. We use the official PyTorch codebase of DDPO, substituting SD-Turbo as the base model. Since SD-Turbo does not support classifier-free guidance or negative prompts, we disable them by setting the guidance scale to 1.0.

REBEL implementation. As REBEL was originally implemented to finetune consistency models [47], we adapt it to finetune SD-Turbo by using the DDPO codebase. For a fair comparison, we keep the shared hyperparameters—such as denoising steps per trajectory, classifier-free guidance scale, learning rate, batch size, and running statistics settings—consistent with DDPO, with REBEL-specific settings derived from the REBEL paper. Unlike DDPO, which generates only one trajectory per batch, REBEL produces a pair of trajectories for reward difference learning. To ensure fair sample rollouts, we halve the number of batches and gradient accumulation steps per epoch for REBEL.

D3PO implementation. Applying D3PO to finetune SD-Turbo is relatively straightforward, as the official D3PO codebase is also built on DDPO. However, for a fair comparison, we still reconfigure certain hyperparameters to align with our DDPO implementation, including denoising steps per trajectory, classifier-free guidance scale, learning rate, and batch size. Like REBEL, D3PO also generates a pair of trajectories per batch for preference learning. Thus, we maintain the same number of batches and gradient accumulation steps per epoch for D3PO as we do for REBEL.

SDPO implementation. Our SDPO setup retains most shared hyperparameters from the REBEL configuration. By leveraging dense rewards, our SDPO removes the need to accumulate full trajectory data, enabling more frequent model updates. To stabilize training under these frequent updates, we reduce the learning rate for our SDPO. Table 2 lists the key hyperparameters for finetuning SD-Turbo [42] with SDPO.

Table 2. SDPO training hyperparameters for Aesthetic Score, ImageReward, HPSv2, and PickScore.

Hyperparameter	Notation	Aesthetic Score	ImageReward	HPSv2	PickScore
Random seed	–	42	42	42	42
Denoising steps per trajectory	T	50	50	50	50
Classifier-free guidance scale	–	1.0	1.0	1.0	1.0
Maximum gradient norm	–	1.0	1.0	1.0	1.0
Optimizer type	–	AdamW	AdamW	AdamW	AdamW
Optimizer weight decay	–	1×10^{-4}	1×10^{-4}	1×10^{-4}	1×10^{-4}
Optimizer β_1	–	0.9	0.9	0.9	0.9
Optimizer β_2	–	0.999	0.999	0.999	0.999
Optimizer epsilon	–	1×10^{-8}	1×10^{-8}	1×10^{-8}	1×10^{-8}
Learning rate	–	1×10^{-4}	5×10^{-5}	5×10^{-5}	6×10^{-5}
Sampling batch size per GPU	B_1	8	8	8	8
Sampling batches per epoch	–	4	4	4	4
Running statistics buffer size	–	32	32	32	32
Running statistics minimal count	–	16	16	16	16
Training batch size per GPU	B_2	2	1	1	1
Gradient accumulation steps	–	8	32	32	16
Log-ratio scale factor	η	1.0	1.0	1.0	1.0
Clipping range	ϵ	1×10^{-4}	1×10^{-4}	1×10^{-4}	1×10^{-4}
Discount factor	γ	0.99	0.99	0.99	0.99
Decay rate	λ	0.99	0.99	0.99	0.99

Experimental environments. Our main experiments in Secs. 4.2 and 4.3 were conducted using the following hardware and software environments:

- GPUs: GeForce RTX 3090 \times 4
- Python 3.10.12
- Numpy 1.26.1

- Diffusers 0.17.1
- Accelerate 0.17
- PyTorch 2.0.1
- Transformers 4.30.2

Training prompts. In Sec. 4, we utilized a set of 45 animal names as training prompts, listed as follows:

cat	dog	horse	monkey	rabbit	zebra	spider	bird	sheep	deer
cow	goat	lion	tiger	bear	raccoon	fox	wolf	lizard	beetle
ant	butterfly	fish	shark	whale	dolphin	squirrel	mouse	rat	snake
turtle	frog	chicken	duck	goose	bee	pig	turkey	fly	llama
camel	bat	gorilla	hedgehog	kangaroo					

A.2. Additional Setup for Consistency Models

For finetuning the latent consistency model [28], we utilize RLCM [34] as the baseline. As the official RLCM codebase integrates both DDPO and REBEL, we adapt only our SDPO to it, aligning key hyperparameters with those of REBEL, except for the SDPO-specific ones (e.g., discount factor, decay rate, and clipping range), which follow the settings in Tab. 2.

B. Instability of Prior Methods in Finetuning with Few-Step Trajectories

Building on the discussion in Sec. 3.1, we further analyze the instability that arises when using prior methods (DDPO [1], REBEL [9], and D3PO [55]) to finetune SD-Turbo with denoising trajectories that contain extremely few steps (e.g. 1 or 2 steps). Figure 7 presents the learning curves of DDPO, REBEL, and D3PO when finetuning SD-Turbo [42] with 1-step and 2-step denoising trajectories, underscoring their difficulties in achieving stable convergence under few-step configurations. Specifically, each of these methods struggles to maintain stable reward optimization in these scenarios, with some exhibiting significant reward collapse due to the diminished quality of low-step samples. Therefore, relying solely on low-quality, low-step samples for finetuning is less informative and can lead to suboptimal updates, reducing the overall effectiveness and stability of the training process. Additionally, Figure 7 also shows the learning curves of DDPO when mixing trajectories of varying lengths during training, where the increased variance across trajectories further contributes to instability.

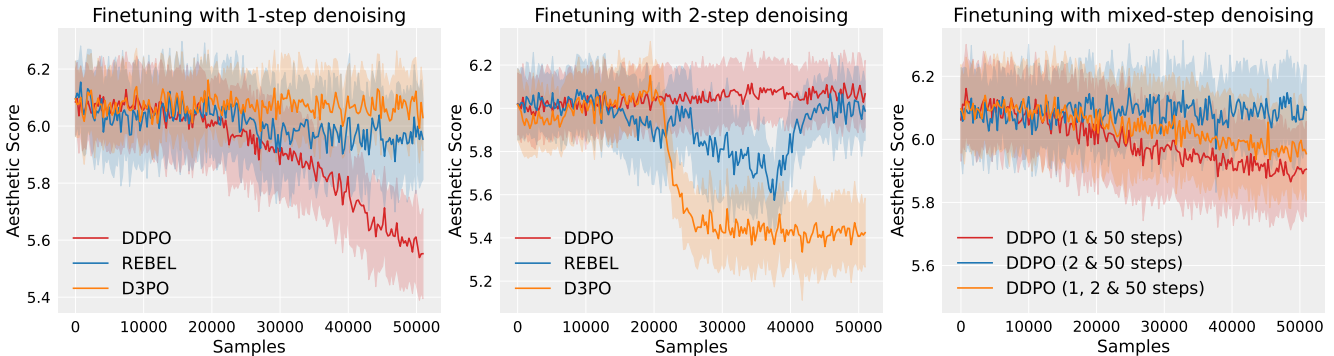


Figure 7. Analysis of the instability of prior methods in finetuning with few-step trajectories. We present the learning curves of DDPO, REBEL, and D3PO during finetuning SD-Turbo with **1-step** (*left*) and **2-step** (*middle*) denoising trajectories, as well as the learning curves of DDPO during finetuning with **mixed-step** trajectories (*right*).

Instead of using mixed-length trajectories with high variance and few-step trajectories with low-quality samples, our SDPO utilizes high-quality intermediate samples from longer, uniform-length trajectories as reliable references. By incorporating dense reward feedback, it ensures robust and stable reward optimization across all denoising steps.

C. Analysis of Similarity Between Predicted and Target Rewards

To further validate the effectiveness of our dense reward prediction approach, we analyze the similarity between the dense rewards predicted by our method, the alternative strategies introduced in our ablation study (Sec. 4.3), and the reward signals directly computed from the target reward function across full trajectories. In Tab. 3, we report three metrics—cosine similarity, L1 distance, and L2 distance—to evaluate the similarity between predicted and target rewards across the following reward functions: Aesthetic Score [43], ImageReward [54], HPSv2 [51], and PickScore [17]. To account for variations in the scale of different reward functions, all reward scores are normalized before similarity computation. Compared with the alternative strategies, our approach (*3 queries & similarity & adaptive anchor*) consistently achieves higher cosine similarity and lower L1/L2 distances across all reward functions. This highlights the effectiveness of our dense reward predictions in approximating the target reward signals, further demonstrating its potential for more precise and reliable model optimization.

Table 3. Similarity between predicted and target rewards.

Reward Function	Method	Cosine Similarity \uparrow	L1 Distance \downarrow	L2 Distance \downarrow
Aesthetic Score	1 query & copy	2×10^{-8}	11630	131
	2 queries & interpolation	0.3368	11228	130
	2 queries & similarity	0.3861	9771	125
	3 queries & similarity & fixed anchor	0.3654	9832	127
	3 queries & similarity & random anchor	0.3561	9744	128
	3 queries & similarity & adaptive anchor	0.4463	9073	119
ImageReward	1 query & copy	2×10^{-8}	11262	130
	2 queries & interpolation	0.3901	10561	125
	2 queries & similarity	0.4078	9340	123
	3 queries & similarity & fixed anchor	0.3611	9423	128
	3 queries & similarity & random anchor	0.3924	9337	125
	3 queries & similarity & adaptive anchor	0.4683	8598	117
HPSv2	1 query & copy	3×10^{-8}	11411	129
	2 queries & interpolation	0.3696	10798	127
	2 queries & similarity	0.3676	9915	127
	3 queries & similarity & fixed anchor	0.3253	9886	131
	3 queries & similarity & random anchor	0.3648	9955	128
	3 queries & similarity & adaptive anchor	0.4549	9009	118
PickScore	1 query & copy	3×10^{-8}	11540	131
	2 queries & interpolation	0.4307	10237	121
	2 queries & similarity	0.4117	9318	123
	3 queries & similarity & fixed anchor	0.3933	9368	125
	3 queries & similarity & random anchor	0.3846	9324	126
	3 queries & similarity & adaptive anchor	0.4853	8657	115

D. Derivations

D.1. The Gradient of the SDPO Objective

As outlined in Eq. (14), Eq. (15), and Eq. (16), the SDPO objective incorporates several components with specific forms of stepwise weighting and clipping. In the following, we derive the gradients for each of these equations. Firstly, the unclipped objective, presented in Eq. (14), is given by:

$$l_\theta(\mathbf{x}_t^a, \mathbf{x}_t^b, \mathbf{c}) = \mathbb{E}_{\mathbf{x}_t^a, \mathbf{x}_t^b, \mathbf{c}} \left[\left(\Delta \rho_t(\theta) \cdot \frac{\lambda^{(T-t-1)}}{\eta} - \Delta \hat{A}_t \right)^2 \right], \quad (17)$$

where $\Delta \rho_t(\theta) := \rho_t^a(\theta) - \rho_t^b(\theta)$ is the difference in log-likelihood ratios, and $\Delta \hat{A}_t := \hat{A}_t^a - \hat{A}_t^b$ is the difference in advantage estimates for trajectories a and b at step t . The gradient of l_θ w.r.t. θ is:

$$\nabla_\theta l_\theta(\mathbf{x}_t^a, \mathbf{x}_t^b, \mathbf{c}) = \mathbb{E}_{\mathbf{x}_t^a, \mathbf{x}_t^b, \mathbf{c}} \left[2 \left(\Delta \rho_t(\theta) \cdot \frac{\lambda^{(T-t-1)}}{\eta} - \Delta \hat{A}_t \right) \cdot \frac{\lambda^{(T-t-1)}}{\eta} \cdot \nabla_\theta \Delta \rho_t(\theta) \right]. \quad (18)$$

To expand $\nabla_\theta \Delta \rho_t(\theta)$, we note that:

$$\nabla_\theta \Delta \rho_t(\theta) = \nabla_\theta \rho_t^a(\theta) - \nabla_\theta \rho_t^b(\theta), \quad (19)$$

where each $\rho_t^j(\theta)$ has a gradient given by:

$$\nabla_\theta \rho_t^j(\theta) = \frac{\nabla_\theta p_\theta(\mathbf{x}_t^j | \mathbf{c})}{p_\theta(\mathbf{x}_t^j | \mathbf{c})}. \quad (20)$$

Substituting it back, we obtain the full gradient for the unclipped objective:

$$\nabla_\theta l_\theta(\mathbf{x}_t^a, \mathbf{x}_t^b, \mathbf{c}) = \mathbb{E}_{\mathbf{x}_t^a, \mathbf{x}_t^b, \mathbf{c}} \left[2 \left(\Delta \rho_t(\theta) \cdot \frac{\lambda^{(T-t-1)}}{\eta} - \Delta \hat{A}_t \right) \cdot \frac{\lambda^{(T-t-1)}}{\eta} \cdot \left(\frac{\nabla_\theta p_\theta(\mathbf{x}_t^a | \mathbf{c})}{p_\theta(\mathbf{x}_t^a | \mathbf{c})} - \frac{\nabla_\theta p_\theta(\mathbf{x}_t^b | \mathbf{c})}{p_\theta(\mathbf{x}_t^b | \mathbf{c})} \right) \right]. \quad (21)$$

To stabilize updates, we constrain the log-likelihood ratios within a trust region by clipping them, yielding the clipped objective in Eq. (15):

$$\tilde{l}_\theta(\mathbf{x}_t^a, \mathbf{x}_t^b, \mathbf{c}) = \mathbb{E}_{\mathbf{x}_t^a, \mathbf{x}_t^b, \mathbf{c}} \left[\left(\Delta \tilde{\rho}_t(\theta) \cdot \frac{\lambda^{(T-t-1)}}{\eta} - \Delta \hat{A}_t \right)^2 \right], \quad (22)$$

where $\Delta \tilde{\rho}_t(\theta) := \tilde{\rho}_t^a(\theta) - \tilde{\rho}_t^b(\theta)$ and $\tilde{\rho}_t^j(\theta) := \text{clip}(\rho_t^j(\theta), -\epsilon, \epsilon)$. The gradient for the clipped objective \tilde{l}_θ w.r.t. θ is:

$$\nabla_\theta \tilde{l}_\theta(\mathbf{x}_t^a, \mathbf{x}_t^b, \mathbf{c}) = \mathbb{E}_{\mathbf{x}_t^a, \mathbf{x}_t^b, \mathbf{c}} \left[2 \left(\Delta \tilde{\rho}_t(\theta) \cdot \frac{\lambda^{(T-t-1)}}{\eta} - \Delta \hat{A}_t \right) \cdot \frac{\lambda^{(T-t-1)}}{\eta} \cdot \nabla_\theta \Delta \tilde{\rho}_t(\theta) \right]. \quad (23)$$

Expanding $\nabla_\theta \Delta \tilde{\rho}_t(\theta)$, we have:

$$\nabla_\theta \Delta \tilde{\rho}_t(\theta) = \nabla_\theta \tilde{\rho}_t^a(\theta) - \nabla_\theta \tilde{\rho}_t^b(\theta), \quad (24)$$

where each $\nabla_\theta \tilde{\rho}_t^j(\theta)$ depends on whether $\rho_t^j(\theta)$ is within the clipping range $[-\epsilon, \epsilon]$. Thus, for each term where $\rho_t^j(\theta)$ is clipped, the gradient will be zero:

$$\nabla_\theta \tilde{\rho}_t^j(\theta) = \begin{cases} \nabla_\theta \rho_t^j(\theta), & \text{if } -\epsilon < \rho_t^j(\theta) < \epsilon, \\ 0, & \text{otherwise.} \end{cases} \quad (25)$$

The final SDPO update, as defined in Eq. (16), employs a step-shuffled gradient update strategy and selects the maximum value between the unclipped and clipped objectives. This stepwise update is formulated as:

$$\mathcal{L}_t(\theta) \leftarrow \frac{1}{B} \sum_{i=1}^B \max \left(l_\theta(\mathbf{x}_{\tau_i}^{a,i}, \mathbf{x}_{\tau_i}^{b,i}, \mathbf{c}_i), \tilde{l}_\theta(\mathbf{x}_{\tau_i}^{a,i}, \mathbf{x}_{\tau_i}^{b,i}, \mathbf{c}_i) \right), \quad (26)$$

where τ_i represents the shuffled step indices for the i -th batch. For each gradient update, we use the objective value corresponding to the maximum between l_θ and \tilde{l}_θ for each sample in the batch. The gradient of $\mathcal{L}_t(\theta)$ w.r.t. θ is:

$$\nabla_\theta \mathcal{L}_t(\theta) = \frac{1}{B} \sum_{i=1}^B \max \left(\nabla_\theta l_\theta(\mathbf{x}_{\tau_i}^{a,i}, \mathbf{x}_{\tau_i}^{b,i}, \mathbf{c}_i), \nabla_\theta \tilde{l}_\theta(\mathbf{x}_{\tau_i}^{a,i}, \mathbf{x}_{\tau_i}^{b,i}, \mathbf{c}_i) \right). \quad (27)$$

This final gradient facilitates stable and efficient updates across steps by incorporating both the unclipped and clipped objectives in each stepwise update, selecting the one that better preserves stability at each step.

E. Additional Evaluation Curves for Step Generalization

During the experiments in Sec. 4.2 exploring the step generalization of our model, we evaluated reward scores for images generated with different numbers of denoising steps beyond the 50-step denoised samples used in training. While Fig. 4 shows evaluation curves for 1-step denoising, additional curves for 2-step, 4-step, 8-step, and 16-step denoising are presented in Figs. 8 to 11, respectively. Across all these evaluations, our SDPO consistently demonstrates superior step generalization performance compared to other algorithms.

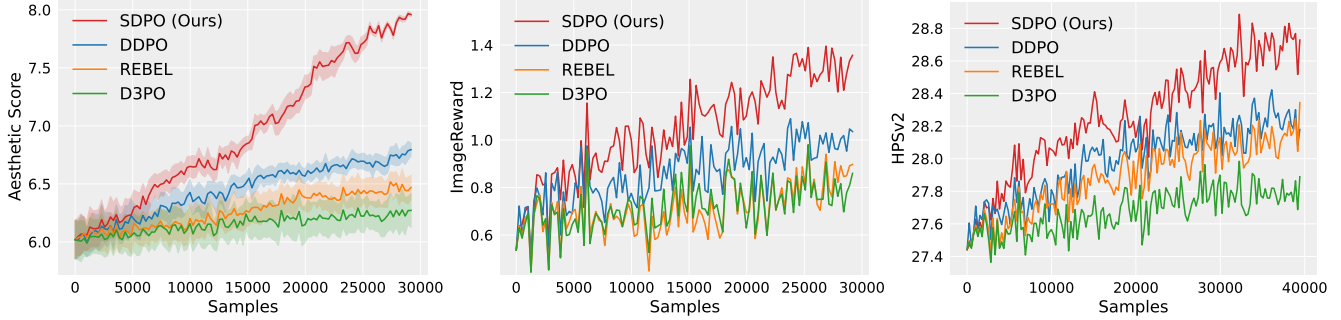


Figure 8. Evaluation curves for generalization to 2-step. Reward scores (left: Aesthetic Score, middle: ImageReward, right: HPSv2) are evaluated for images generated with 2 denoising steps. The horizontal axis represents the cumulative number of training samples.

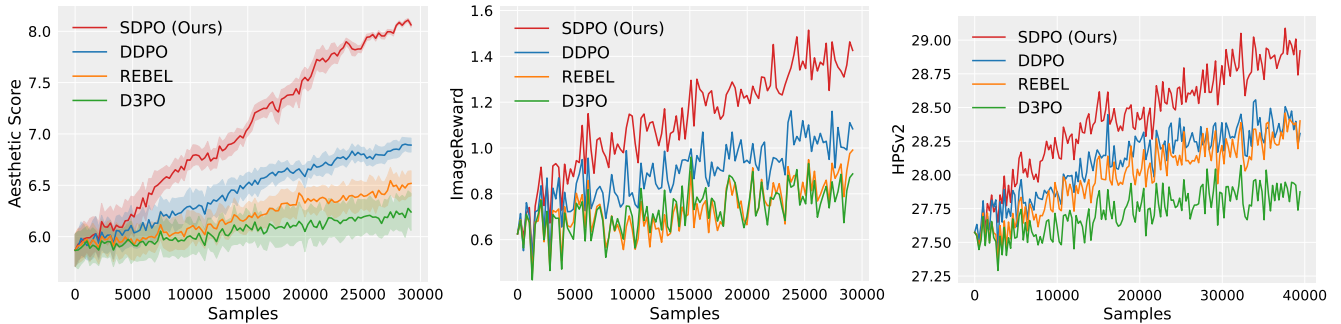


Figure 9. Evaluation curves for generalization to 4-step. Reward scores (left: Aesthetic Score, middle: ImageReward, right: HPSv2) are evaluated for images generated with 4 denoising steps. The horizontal axis represents the cumulative number of training samples.

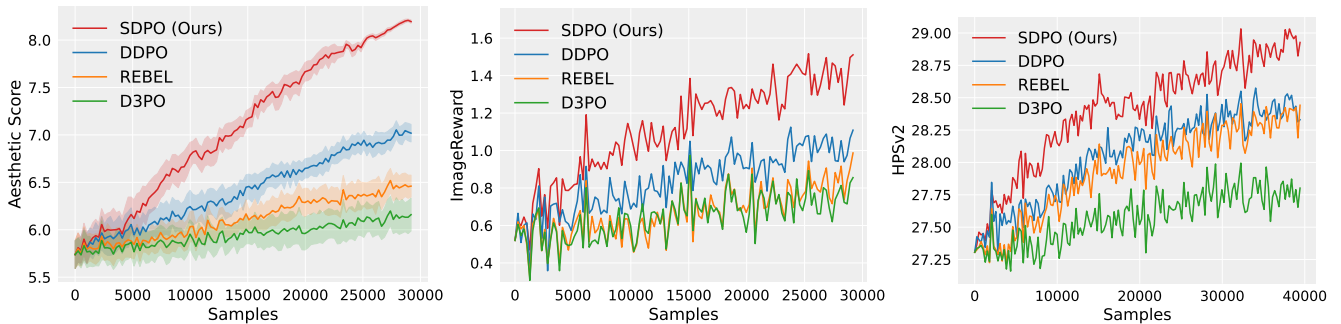


Figure 10. Evaluation curves for generalization to 8-step. Reward scores (left: Aesthetic Score, middle: ImageReward, right: HPSv2) are evaluated for images generated with 8 denoising steps. The horizontal axis represents the cumulative number of training samples.

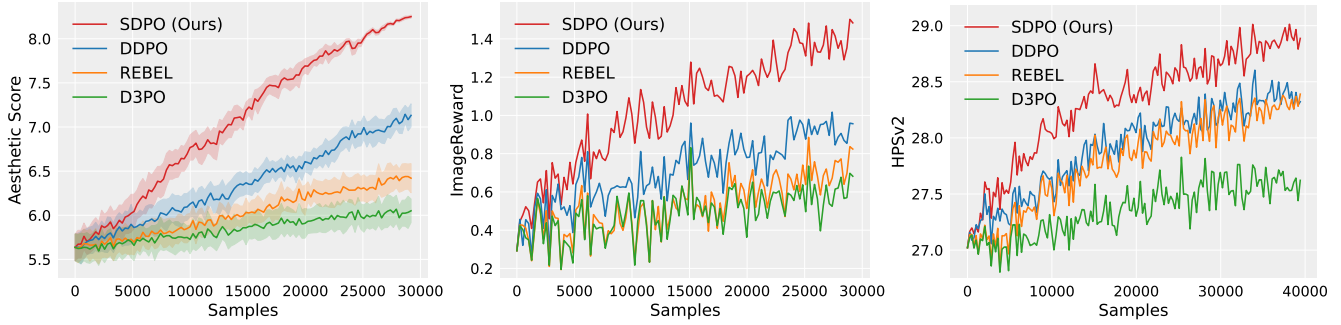


Figure 11. Evaluation curves for generalization to 16-step. Reward scores (left: Aesthetic Score, middle: ImageReward, right: HPSv2) are evaluated for images generated with 16 denoising steps. The horizontal axis represents the cumulative number of training samples.

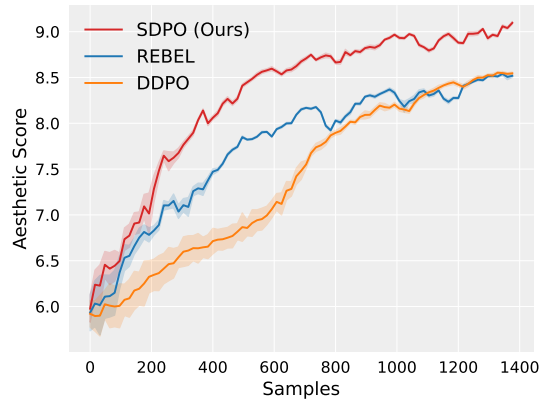
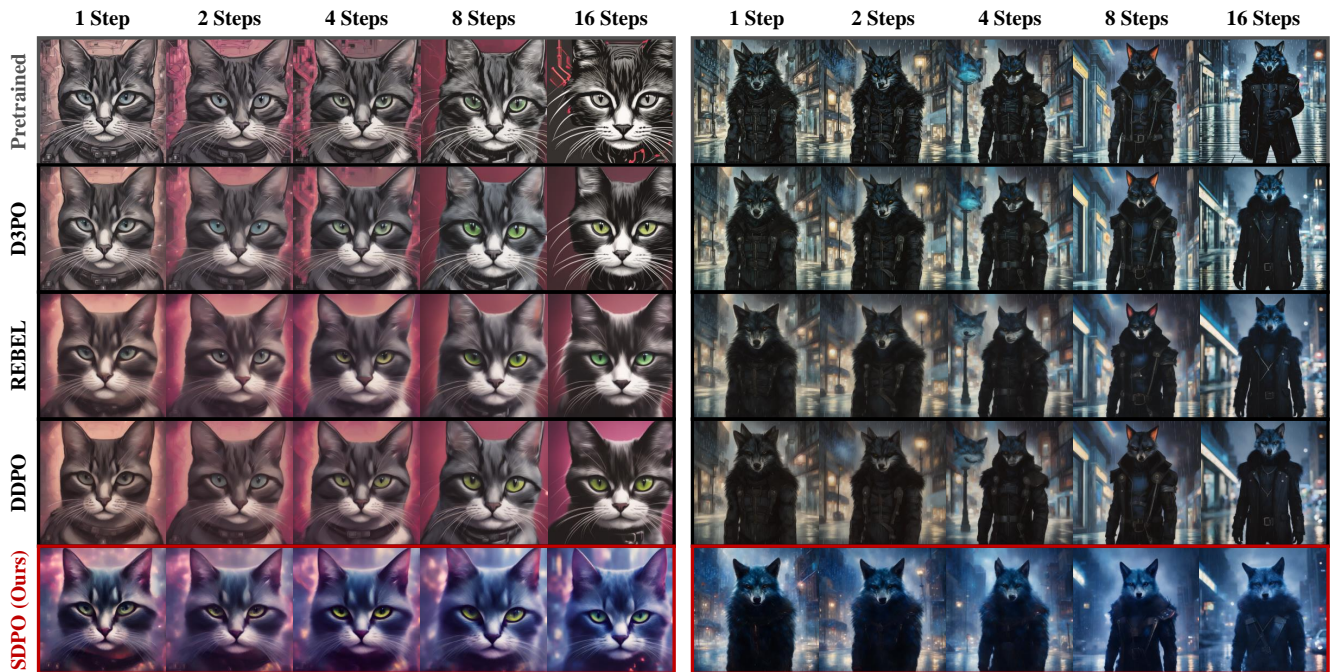


Figure 12. Learning curves for latent consistency model. Our SDPO still outperforms DDPO and REBEL in reward optimization for the latent consistency model.

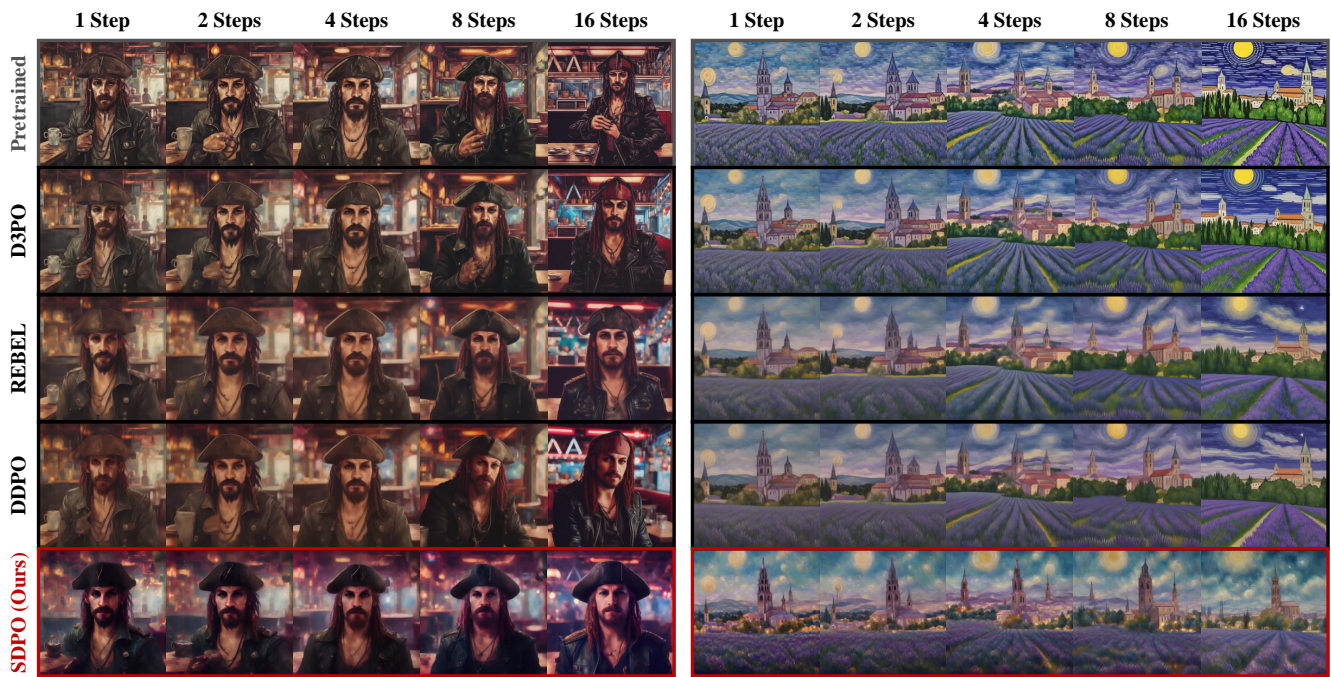
F. Additional Qualitative Examples

In Figs. 13 to 18, we present additional samples from our SDPO, comparing with samples from DDPO, REBEL, D3PO, and pretrained SD-Turbo. While low-step samples from the other methods exhibit lower visual quality and weaker alignment with the target reward structure, our SDPO consistently delivers high-quality, reward-aligned images across all sampling steps.



portrait of a cute cyberpunk cat, realistic, professional

Portrait of a male furry anthro Blue wolf fursona wearing black cyberpunk clothes in a city at night while it rains.



A portrait of a pirate in a cyberpunk cafe setting.

A landscape featuring a lone magic the gathering-style building.

Figure 13. Generated images for unseen prompts by: pretrained SD-Turbo and models finetuned on PickScore, using the same number of training samples during finetuning. All images are generated with the same random seed.

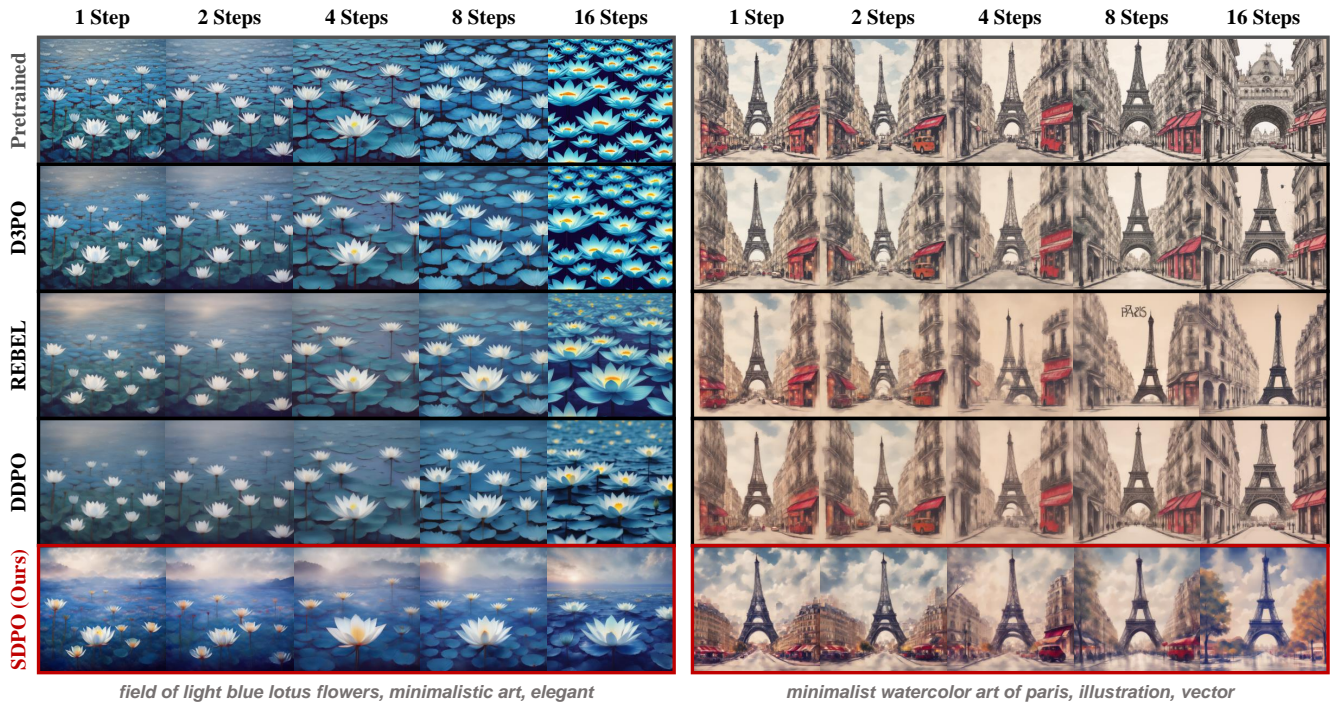


Figure 14. Generated images for unseen prompts by: pretrained SD-Turbo and models finetuned on PickScore, using the same number of training samples during finetuning. All images are generated with the same random seed.

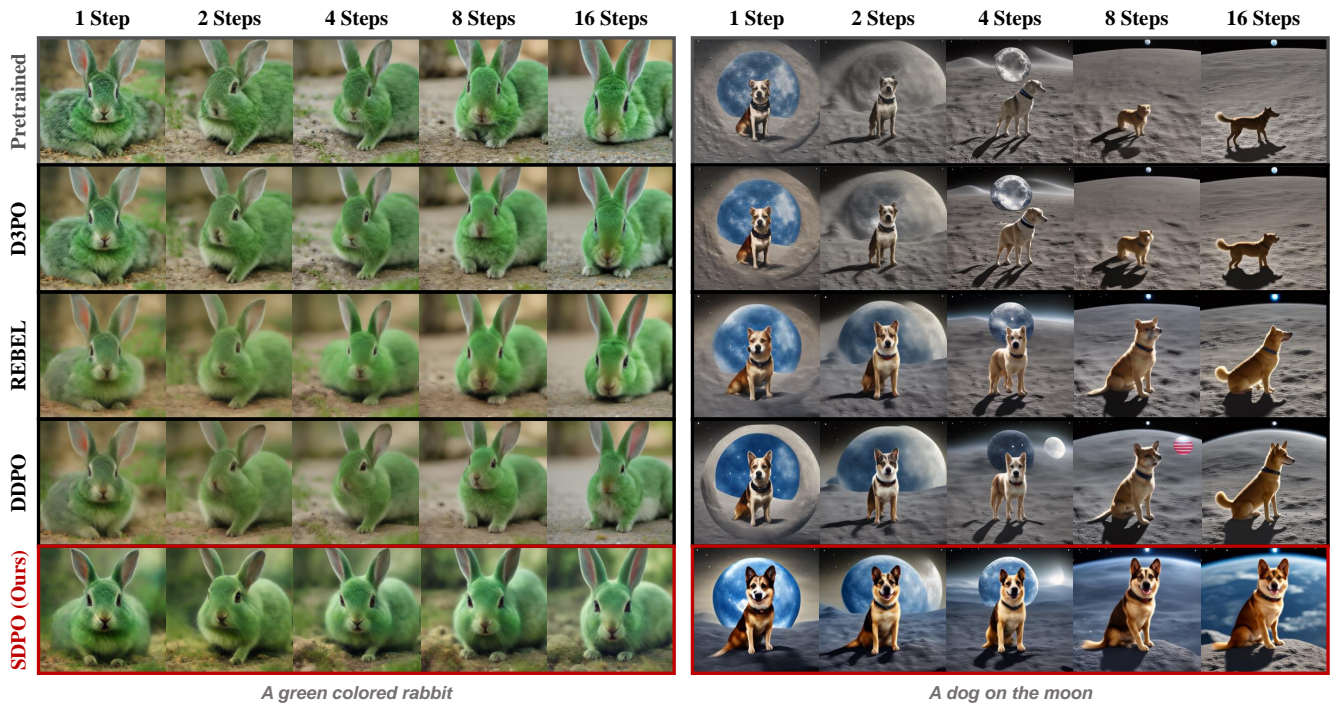


Figure 15. Generated images for unseen prompts by: pretrained SD-Turbo and models finetuned on PickScore (left) and HPSv2 (right), using the same number of training samples during finetuning. All images are generated with the same random seed.

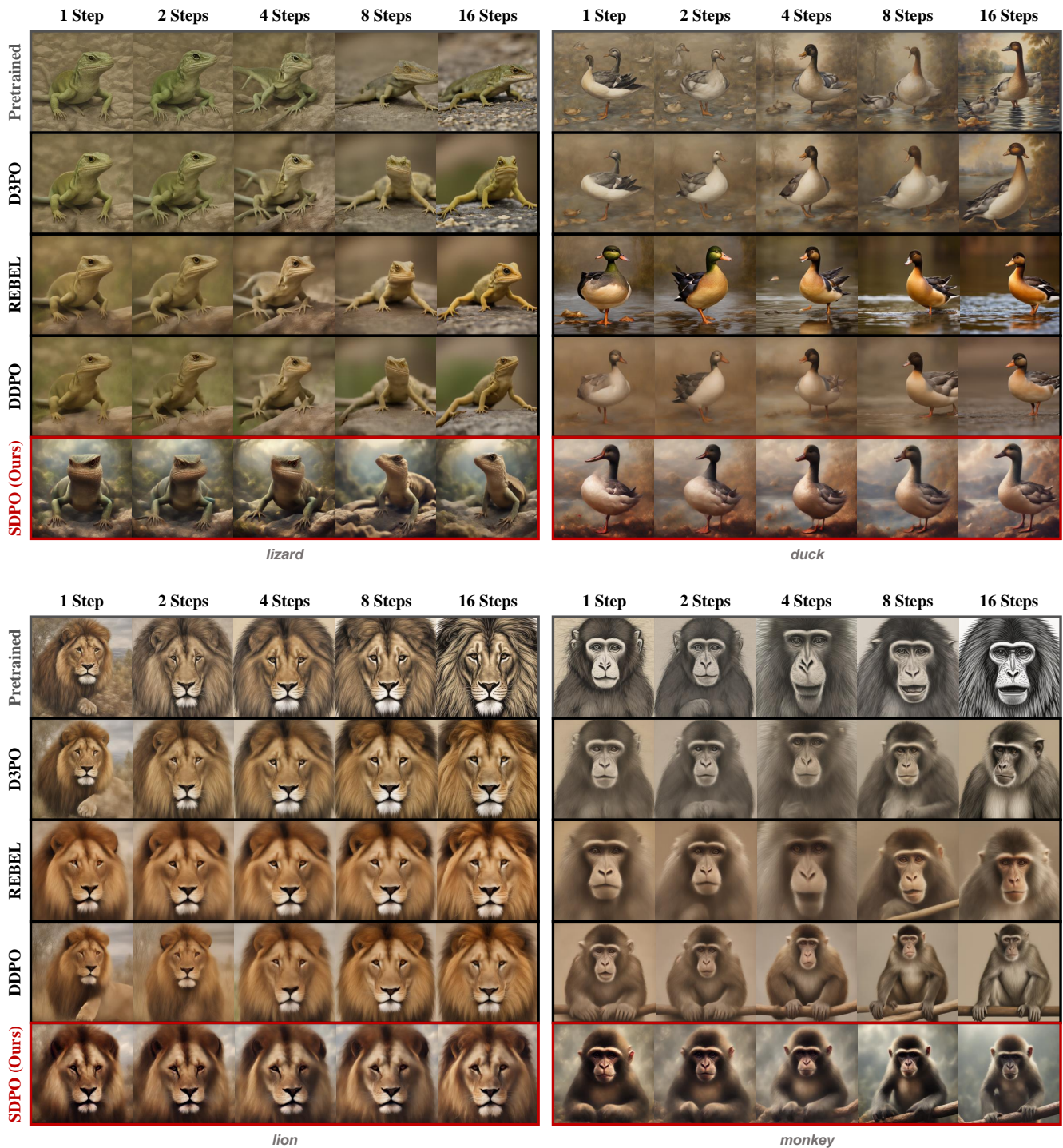


Figure 16. Generated images for seen prompts by: pretrained SD-Turbo and models finetuned on PickScore, using the same number of training samples during finetuning. All images are generated with the same random seed.

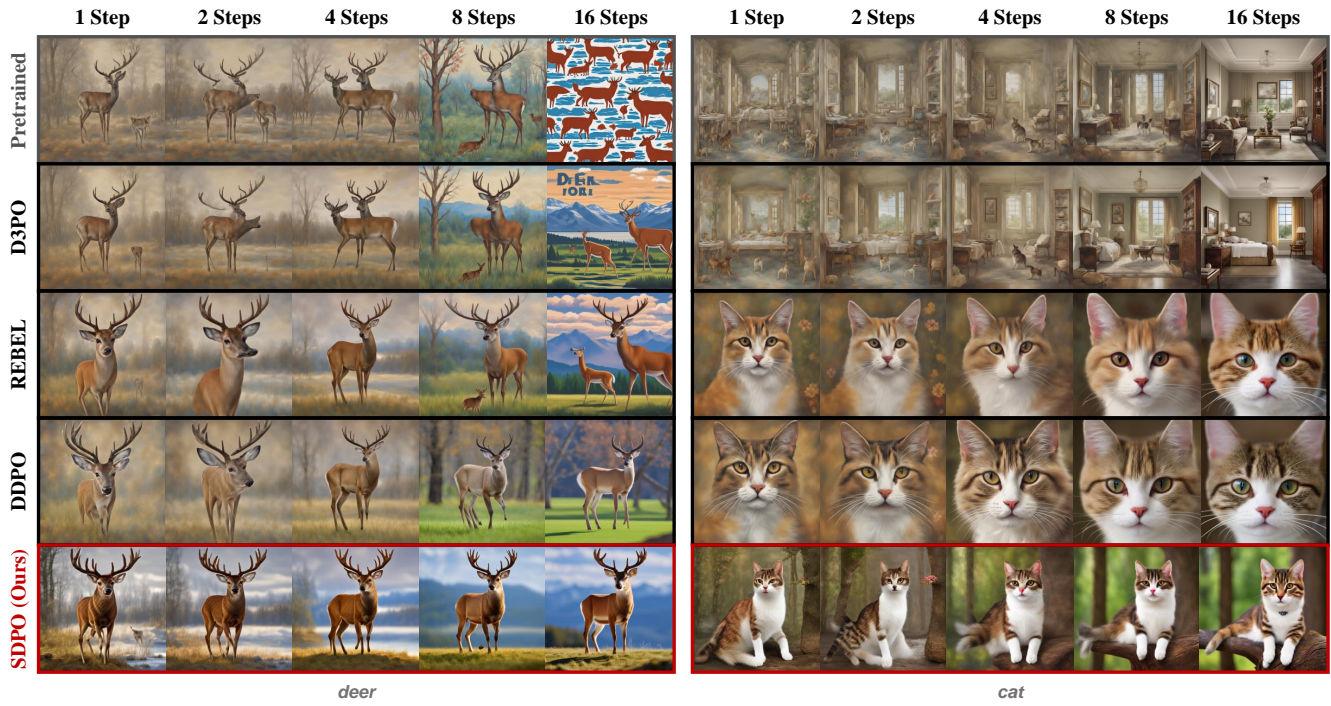


Figure 17. Generated images for seen prompts by: pretrained SD-Turbo and models finetuned on HPSv2, using the same number of training samples during finetuning. All images are generated with the same random seed.

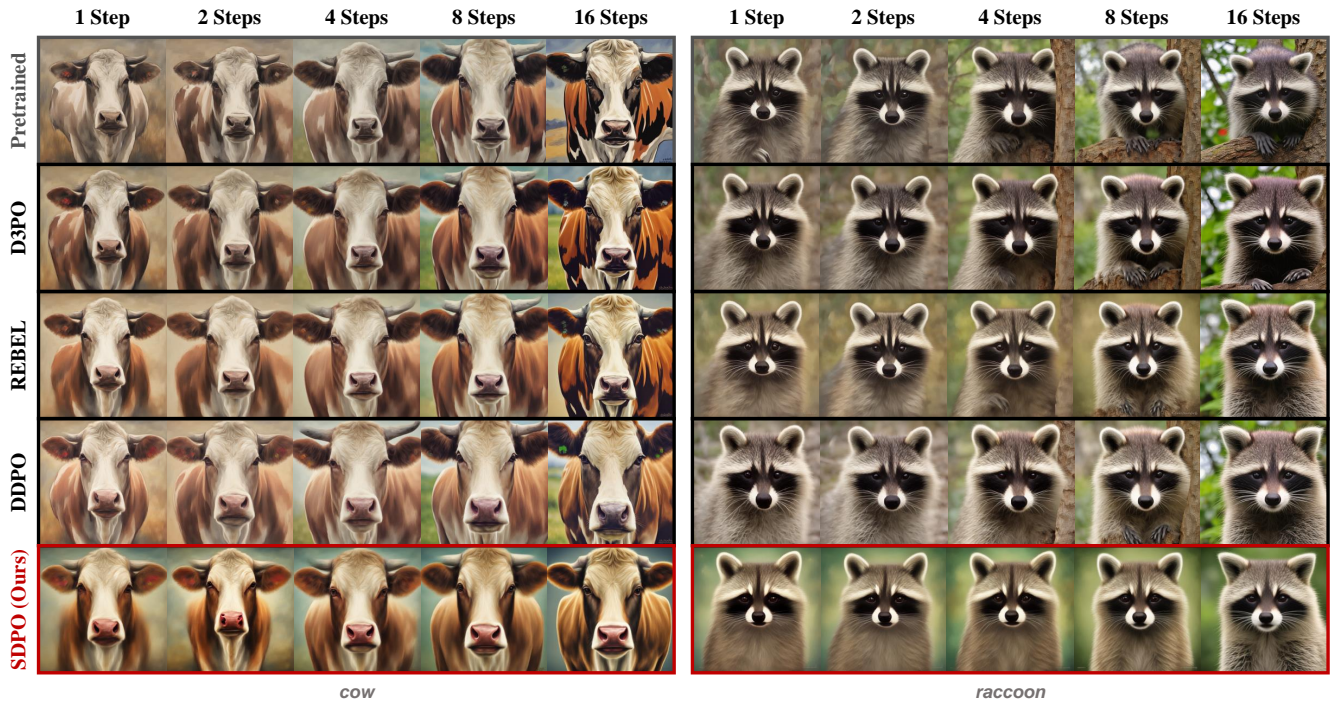


Figure 18. Generated images for seen prompts by: pretrained SD-Turbo and models finetuned on ImageReward, using the same number of training samples during finetuning. All images are generated with the same random seed.